Airborne and Ground Electrical Surveys of the Edwards and Trinity Aquifers, Medina, Uvalde, and Bexar Counties, Texas

By Bruce D Smith[1], David V. Smith[1], Jeffrey G. Paine[2], and Jared D. Abraham[1]
[1]U.S. Geological Survey, MS 964, Box 25046, Denver Federal Center, Denver, CO 80225,
[2]Bureau of Economic Geology, Jackson School of Geological Sciences, The University of Texas at Austin, Univ. Station, Box X, Austin, TX 78713

ABSTRACT

Helicopter electromagnetic (HEM) and magnetic surveys were flown in the Seco Creek area, (Medina and Uvalde Counties, TX, 2002) and in Northern Bexar County (TX, 2003). The purpose of these surveys was to map structure and lithology of the Edwards and Trinity aquifers consisting of the catchment zone (Glen Rose, Trinity Group), recharge zone (Devils River, Edwards Group), and confined zone. The latter survey concentrated on Camps Stanley and Bullis, which are located mostly on the Glenn Rose. The southern part of Camp Bullis includes the faulted contact between the Edwards Group (recharge zone) and the catchment (Glenn Rose).

Ground geophysical surveys at Seco Creek, conducted by the USGS in April 2002, consisted of total field magnetics, dc resistivity and shallow terrain conductivity measurements. In May 2003, BEG (Bureau of Economic Geology) acquired ground electrical conductivity measurements at 379 locations. Re-mapping of the geology along the nine geophysical lines was done at the same time. The shallow ground conductivity interpretations were supplemented by time domain EM (TDEM) soundings by the USGS. Ground-based measurements demonstrate that (a) mapped geologic units consisting of Cretaceous age limestones and dolomitized limestones, marls, mudstones, shales, and Quaternary alluvial deposits have differences in apparent conductivity, (b) geologic structures such as faults and karst can have detectable apparent conductivity signatures, and (c) conductivity measurements can be combined with geologic maps and outcrop studies to identify hidden contacts, covered strata, and unmapped structural features. Limited comparisons of measurements confirm that the ground and airborne geophysical systems produce similar apparent electrical conductivities at comparable frequencies and coil orientation.

The ground based geophysical surveys refine the airborne geophysical data, revealing greater structural complexity than depicted in the original geologic mapping. Ramp structures are well defined by the geophysical surveys including a large complexly breached ramp along Seco Creek. The airborne geophysical data indicate a distinct difference in electrical resistivity between the upper and lower Devils River formations in the recharge area. In addition the electrical data have been used to map the subsurface configuration of upper confining clay units (Del Rio and Eagle Ford). The Glenn Rose formation has a lower resistivity than the Edwards group formations. A previously unknown collapse feature in the study area is inferred from a high resistivity area along Seco Creek in the Trinity Aquifer. Geologic maps of four 7.5-minute quadrangles of the Seco Creek area have been digitized and revised based on the geophysical surveys. The geophysical data has been critical in the construction of a 3D geologic model of the study area because of deficient well data for subsurface information and the extent of colluvium hiding near surface structures and bedrock. Ground geophysical surveys can capture small-scale lateral electrical conductivity changes, complementing smoothed but spatially dense airborne electrical conductivity measurements. Airborne surveys cover large areas that are inaccessible or impractical to survey using ground-based instruments. They also provide aerial detail of the subsurface not available from photo-geologic and other near-surface mapping methods.

Magnetic Geophysical Applications Reveal Igneous Rocks and Geologic Structures in the Edwards Aquifer, Texas

By D.V. Smith[1], C. Foss[2], and B.D. Smith[1] (Authors)
[1]U.S. Geological Survey, Box 25046 MS964, Denver, CO 80225-0046
[2]Encom Technology Pty Ltd, Level 2, 118 Alfred Street, Milsons Point NSW 2061, Australia

ABSTRACT

High-resolution aeromagnetic surveys were completed over the Edwards aquifer in Uvalde and Medina Counties west of San Antonio, Texas. These surveys have provided new information on the geology and structure of one of the most productive and permeable carbonate aquifers in the United States. A regional scale fixed-wing survey, flown in 2001, revealed the widespread occurance of shallow igneous rocks. Geophysical interpretations show many of the magnetic anomalies to be vertical or subvertical volcanic pipes. Other shallow anomalies are interpreted as sills, lava lakes and pyroclastic flows. The absence of dikes and dike-like structures leads to the hypothesis that the emplaced volcanic rocks affect ground water flow locally, but not significantly on a regional scale. The interpreted intrusive boundaries and geometry can be used in regional hydrologic models to evaluate their influence on ground water flow. Deeper seated anomalies are interpreted as magmatic reservoirs that perhaps served as sources for the late-Cretaceous volcanism.

A small scale very high resolution magnetic data set was acquired in 2003 as part of a helicopter electromagnetic survey of the North Seco Creek study area, which is outside the main Uvalde volcanic field. In addition to a single small volcanic pipe, this data set reveals the trace of the Woodard Cave fault, a major normal fault juxtaposing the rocks of the Trinity Group, comprising the upper Trinity aquifer to the north, with the Devils River Formation, constituting the Edwards aquifer to the south. This important finding, that a fault between adjoining limestone units is associated with a linear magnetic low, led to a re-examination of the fixed-wing aeromagnetic data. Through careful microleveling, filtering and image enhancement techniques, we see that major faults of the Balcones fault zone are associated with vestigial magnetic lineaments on a regional scale.

Structural Controls on Karst Development in Fractured Carbonate Rock, Edwards and Trinity Aquifers, South-Central Texas

By Jason R. Faith[1], Charles D. Blome[2], Allan K. Clark[1], George B. Ozuna[1], and Bruce D. Smith[2]
[1] U.S. Geological Survey, San Antonio, TX
[2] U.S. Geological Survey, Denver, CO

ABSTRACT

The Edwards aquifer of south-central Texas lies within, and adjacent to, the Balcones fault zone and is one of the most productive carbonate aquifers in the United States. The Trinity aquifer outcrops to the north of the Balcones fault zone and supplies baseflow to streams flowing south over the Edwards recharge zone. The geology of Edwards and Trinity aquifers consists of approximately 400 meters of Lower Cretaceous carbonates with interbedded marl and dolostone. Miocene age faults within the Balcones fault zone are *en echelon*, exhibiting primarily normal displacement, trending northeast and downthrown to the southeast. Numerous cross-faults oriented perpendicular to the primary faults trend to the southeast. In the Edwards aquifer, cross-faults breach relay ramps between overlapping faults, providing both a mechanical and hydrologic link between the primary faults.

The fracturing within relay ramps and adjacent to the primary faults in the Edwards aquifer is quite variable, resulting in the development of circuitous and prolific ground-water flow paths. Because of the crystalline nature of the host rock and the susceptibility of the carbonate strata to karst formation, the enhancement of secondary porosity and permeability in fracture zones and fault planes is highly likely in both the Edwards and Trinity aquifers. Vertical displacement of the terrain from north to south by Balcones faults allows for steep hydraulic gradients to develop, maintaining high flow velocities of meteoric groundwater in the shallow sub-surface during recharge events. This process of karst formation resulting from the dissolution of fractures and enhancement of fracture zone permeability occurs primarily parallel to the down-dip direction, along high-angle cross-faults and fracture zones that trend nearly perpendicular to the regional ground-water flow direction. In both the Edwards and Trinity aquifers, a relation between fractures and faults and their susceptibility to dissolution by groundwater can often be observed in outcrop as recrystallized calcite or cavities filled with oxidized clays.

Mapping in the Edwards and Trinity aquifer region in south-central Texas reveals a bimodal distribution of fracture zones and faults and corresponding cave passages oriented both parallel and nearly perpendicular to the northeast-trending, primary faults. The most well-developed caves and solution zones are not aligned with the major faults, but are oriented along the northwest to southeast trend of cross-faults and shorter fracture zones, that parallel the down-dip direction of the Balcones fault zone, and are nearly perpendicular to regional ground-water flow direction. The location and extent of most sensitive karst features in the region are unmapped and those that are have not been released to the public. However, the fracture zones and faults that influence the location and direction of secondary porosity development have been mapped; thus providing a representative surface expression of potential zones of karst enhanced fractures and highly developed cavern systems. Understanding the relation between these fracture zones/faults and the subsequent karst development can assist in the identification and quantification of high volume, high velocity ground-water flow paths in the Edwards and Trinity aquifers.

Simulating Ground-Water Flow in the Karstic Madison Aquifer using a Porous Media Model

By L.D. Putnam and A.J. Long
U.S. Geological Survey, 1608 Mountain View Road, Rapid City, South Dakota, 57702

Ground-water flow in karstic aquifers is characterized by the preferential solution enlargement of fractures and openings creating an integrated network of conduits with rapid flow. Although these conduits can be a predominant feature in characterizing ground-water flow, ground-water storage may occur primarily in the surrounding diffuse network of fractures and smaller openings. A porous media model can provide a reasonable approximation of ground-water flow in the diffuse network; however, simulation of conduit flow in conjunction with the diffuse flow is more problematic. Combinations of heterogeneity, anisotropy, flow barriers, and multiple model layers were used to simulate diffuse and conduit ground-water flow in the karstic Madison Limestone near Rapid City, South Dakota. The finite-difference MODFLOW model included 140 rows, 110 columns, and 5 layers. Cells were 492 feet on a side in the Rapid City area and increased to 6,562 feet near the perimeter of the model. Transient calibration included a 10-year period with 20 stress periods of 6 months. Layers 3 and 4 represented the Madison Limestone with layer 3 representing the upper part of the formation that generally contains more karst features than the less permeable lower part of the formation. Layers1 and 2 represented the overlying Minnelusa Formation, and layer 5 represented the underlying Deadwood Formation. High velocity flowpaths in the Madison Limestone were simulated with conduit zones in layer 3 that were about 1,500 feet wide. Hydraulic conductivities within these zones ranged from about 65 to 1,150 feet/day compared to an average for the surrounding area of about 35 feet per day. The average hydraulic conductivity of layer 4 was 0.32 feet/day. Anisotropy ratios aligned with the high velocity flowpaths ranged from 5:1 to 20:1. The Modflow horizontal flow barrier package was used to simulate the hydrologic effect of a fault. Ground-water tracer studies, transient hydraulic heads, and springflow measurements were used to calibrate the model. Simulated ground-water velocities for high velocity flowpaths were about 500 to 1,000 feet/day compared to observed dye tracer velocities that ranged from about 1,000 to 5,000 feet/day. For the transient simulation, the average difference between observed and simulated hydraulic heads for 269 measurements was 7 feet and the average absolute difference was 31 feet. Linear regression of the observed and simulated hydraulic heads had an R^2 of 0.92. Observed average springflow for the transient period was 21.6 cubic feet per second compared to simulated average springflow of 20.4 cubic feet per second.

Dual Conductivity Module (DCM), A MODFLOW Package for Modeling Flow in Karst Aquifers

By Scott L. Painter, Ronald T. Green, and Alexander Y. Sun
Geosciences and Engineering Division, Southwest Research Institute, 6220 Culebra Road, San Antonio, Texas, 78238

ABSTRACT

A MODFLOW module, DCM, has been developed to better represent the dynamic, multiple time-scale hydraulic response of karst aquifers. DCM adopts a dual-conductivity approach in which the aquifer is conceptualized as being composed of two interacting flow systems - a highly transmissive conduit system embedded in a relatively low permeability diffuse flow system. This coupled-system conceptualization allows not only water levels, but also aquifer dynamics related to rapid conduit flows to be represented. The conduit system may be modeled as a pervasive (continuum) system or as a sparse network of individual conduits, depending on the scale of investigation and the nature of the karst system being investigated. Conduits may be partially or fully filled with water, and transitions between the partially filled and fully filled states are accommodated, which makes it possible to model highly complex hydraulic responses. Flow in the conduit system may be turbulent, laminar, or transitional. Our preliminary results show improved match to both water level measurements and spring discharges records.

Conceptualization and Simulation of the Edwards Aquifer, San Antonio Region, Texas

By R.J. Lindgren[1], A.R. Dutton[2], S.D. Hovorka[3], S.R.H. Worthington[4], and Scott Painter[5]

[1] U.S. Geological Survey, 5563 De Zavala Road, Suite 290, San Antonio, TX 78249

[2] The University of Texas at San Antonio, Department of Earth and Environmental Sciences, 6900 N. Loop 1604 W., San Antonio, TX 78249

[3] The University of Texas at Austin, Bureau of Economic Geology, John A. and Katherine G. Jackson School of Geosciences, University Station, Box X, Austin, TX 78713

[4] Worthington Groundwater, 55 Mayfair Avenue, Dundas, Ontario, Canada, L9H 3K9

[5] Southwest Research Institute, 6220 Culebra Road, San Antonio, TX 78238

ABSTRACT

A new numerical ground-water-flow model (Edwards aquifer model) that incorporates important components of the latest information and a conduit-flow dominated conceptualization of the Edwards aquifer was developed. The conceptualization emphasizes conduit development and conduit flow, as opposed to predominately diffuse, porous-media flow. The model incorporates conduits simulated as generally continuously connected, one-cell-wide (1,320 feet) zones with very large hydraulic-conductivity values (as much as 300,000 feet per day). The locations of the conduits are based on a number of factors, including major potentiometric-surface troughs in the aquifer, the presence of sinking streams, geochemical information, and geologic structures (for example, faults and grabens).

The model includes both the San Antonio and Barton Springs segments of the Edwards aquifer in the San Antonio region, Texas, and was calibrated for steady-state (1939–46) and transient (1947–2000) conditions. Transient simulations were conducted using monthly recharge and pumpage (withdrawals) data. The root mean square errors for hydraulic heads represent about 4 to 8 percent of the total head differences across the model area. The root mean square errors for Comal, San Marcos, San Antonio, and San Pedro Springs, as a percentage of the range of discharge fluctuations measured at each of the springs, are less than 10 percent.

The simulated directions of flow in the Edwards aquifer model are most strongly influenced by the presence of simulated conduits and barrier faults. The simulated conduits tend to facilitate flow. The simulated subregional flow directions generally are toward the nearest conduit and subsequently through and parallel to the conduits from the recharge zone into the confined zone and toward the major springs. Structures simulated in the Edwards aquifer model that tend to restrict ground-water flow are barrier faults. The influence of simulated barrier faults on flow directions is most evident in northern Medina County.

INTRODUCTION

The Edwards aquifer in the Balcones fault zone of south-central Texas (fig. 1) is one of the most permeable and most productive aquifers in the world. The sole source of drinking water supply in the San Antonio and Austin areas, the aquifer is critical to farming and ranching economies west of San Antonio and recreational economies northeast of the city. There is also concern that drought or the increasing demand for ground water, or both, might result in the deterioration of habitats for several endangered species. To evaluate the hydrologic response to various alternative proposals for managing the Edwards aquifer in the San Antonio region, the Edwards Aquifer Authority (EAA), together with other San Antonio water-resource managers and planners, expressed the need for an improved numerical ground-water-flow model. As a result of this need, a study was conducted from 2000 to 2003 by the U.S. Geological Survey (USGS) and The University of Texas at Austin, Bureau of Economic Geology

(BEG), in cooperation with the U.S. Department of Defense (DOD) and the EAA; and a numerical ground-water-flow model was developed (Lindgren and others, 2004).

CONCEPTUALIZATION OF THE EDWARDS AQUIFER

The conceptualization of the Edwards aquifer presented in Lindgren and others (2004) emphasizes conduit development and conduit flow. The degree to which conduits pervade the Edwards aquifer and influence ground-water flow remains controversial, however. An alternate conceptualization, which can be called the diffuse-flow conceptualization, reflects the hypothesis that, although conduits likely are present, flow in the aquifer predominately is through a network of small fractures and openings sufficiently numerous that the aquifer can be considered a porous-media continuum at the regional scale. Whether conduit flow or diffuse flow predominates at the regional scale is an open question.

The Edwards aquifer is part of an aquifer system developed in thick and regionally extensive Lower Cretaceous carbonates that underlie large areas of Texas. The gentle southeastward dip of Cretaceous strata in the Edwards Plateau and Hill

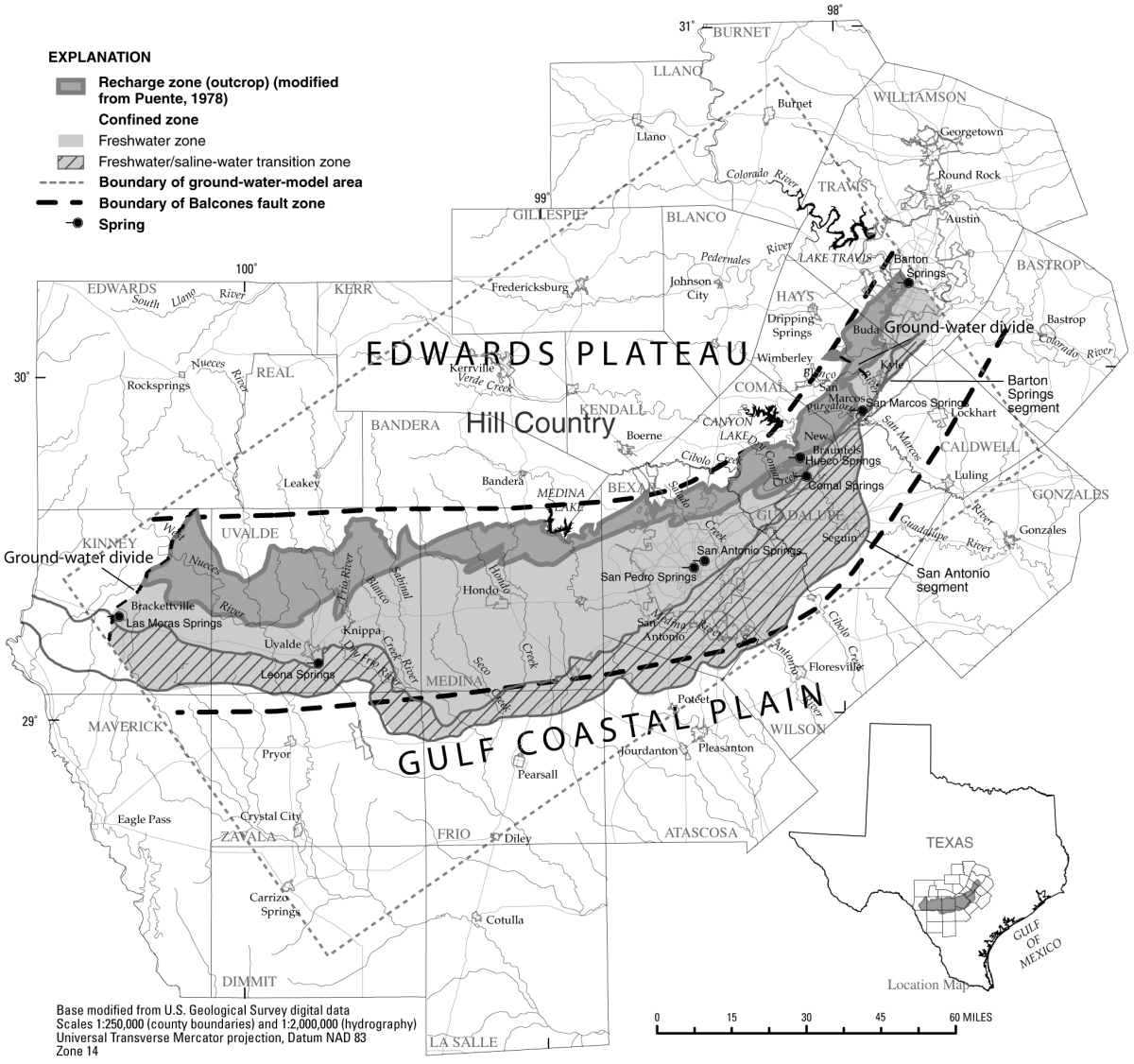

Figure 1. Location of hydrogeologic zones, ground-water-flow model area, and physiographic regions, San Antonio region, Texas.

Country is interrupted across the Balcones fault zone by a system of en echelon faults that generally strike northeastward (Maclay, 1995). The Edwards aquifer is unconfined adjacent to and in the outcrop (recharge zone) and confined in downdip parts of the Balcones fault zone by overlying hydrogeologic units of small to very small permeability. The confined zone of the aquifer is defined on its downdip (gulfward) margin by a freshwater/saline-water transition zone of brackish water. The aquifer thickness in the confined zone ranges from about 450 feet (ft) near the recharge zone in Bexar, Comal, and Hays Counties to about 1,100 ft in Kinney County.

Permeability in the Edwards aquifer includes matrix, fracture, and conduit permeability, varies more than eight orders of magnitude, and is multimodal with distinct but overlapping data populations (Hovorka and others, 1998). Mean hydraulic conductivity of the confined zone (34 feet per day [ft/d]) is more than 120 times greater than mean hydraulic conductivity in the unconfined, or recharge, zone (0.28 ft/d) (Hovorka and others, 1998). Vertical variations in permeability in the Edwards aquifer indicate that the entire aquifer is highly permeable, as well as highly variable. Painter and others (2002) estimated hydraulic conductivity for the Edwards aquifer in the San Antonio region using a combination of spatial statistical methods and advanced techniques for automatic model calibration. The estimated hydraulic conductivity ranges from less than or equal to 20 to 7,347 ft/d. Hovorka and others (1998) reported that transmissivity ranges from 10^{-1} to 10^{7} feet squared per day (ft^2/d), and hydraulic conductivity ranges from 10^{-3} to 10^{5} ft/d, on the basis of specific-capacity and other aquifer tests.

Evidence of the karstic nature of the Edwards aquifer includes outcrop evidence, subsurface data, hydrologic evidence, and tracer tests. More than 400 caves have been inventoried in the Edwards outcrop (Veni, 1988; Elliott and Veni, 1994). Hovorka and others (1998) reported that in two-dimensional cross section, karst features make up 1 to 5 percent of the area of the outcrop. The existence of karst in the deep-subsurface saturated zone is known from borehole televiewer images of caves and solution-enlarged fractures, cave textures and sediments recovered in cores, bit drops during well construction, and oversize caliper logs and off-scale porosity logs.

Evidence of karst flow in the Edwards aquifer is the heterogeneous and rapidly responsive nature of water-level variation. Water levels in the aquifer and discharge at springs rise rapidly after rainfall and then decline at a variable rate, showing drainage from rocks characterized by both conduits and matrix permeability (Atkinson, 1977). Wells close together can have different responses to a single recharge pulse (Johnson and others, 2002). Tomasko and others (2001) and Worthington (2004) documented rapid spring response to rainfall. Tracer testing that began in the San Antonio segment of the Edwards aquifer has shown rapid flow from wells to the nearby high-flow springs (Ogden and others, 1986; Schindel and others, 2002).

A regionally extensive system of high-permeability zones (conduits) is defined by broad troughs in the potentiometric surface in the confined zone of the Edwards aquifer (Hovorka and others, 2004; Worthington, 2004). Particularly favorable locations for development of conduits are in grabens and synclines (Worthington, 2004). In addition, high porosity and permeability in the deepest parts of the aquifer near the freshwater/saline-water transition zone, anomalously high well yields, and sharp chemical gradients all indicate that conduit development and flow might be focused in this area.

The primary source of recharge to the Edwards aquifer is provided by seepage from streams crossing the outcrop area (recharge zone). Estimates of the combined recharge to the San Antonio segment of the Edwards aquifer from stream seepage and infiltration of rainfall range from a low of 43,700 acre-feet (acre-ft) during 1956 to a high of 2,486,000 acre-ft during 1992 (Hamilton and others, 2003). The Edwards aquifer in many areas in the Balcones fault zone is juxtaposed against the Trinity aquifer, both at the surface and at depth; therefore, the Trinity aquifer likely discharges directly into the Edwards aquifer. Estimates of this flow range from 2 percent (LBG-Guyton Associates, 1995) to 9 percent (Mace and others, 2000) of the average estimated annual recharge to the Edwards aquifer.

Most discharge from the Edwards aquifer occurs as: (1) springflow and (2) withdrawals by industrial, irrigation, and public-supply wells. Springflow totaled 69,800 acre-ft during the 1950s drought and reached a record high of 802,800 acre-ft in 1992 (Hamilton and others, 2003). Comal and San Marcos Springs are the largest springs, with total discharges of 274,800 and 195,900 acre-ft, respectively, in 2002 (Hamilton and others, 2003). Total ground-water withdrawals by wells increased steadily at an average annual rate of about 4,500 acre-feet per year (acre-ft/yr), more than tripling between 1939 and 2000.

Water levels in the Edwards aquifer do not show a long-term decline as a result of ground-water withdrawals. The aquifer is dynamic, with water levels generally responding to temporal variations in recharge and spatial distributions of ground-water withdrawals. During periods of drought, water levels decline, but recover rapidly in response to recharge. The drought of the early 1950s is documented in well hydrographs by the downward trends of water levels at these wells. The highest water levels occurred in the early 1990s.

Karstic conduits are major contributors of flow in the Edwards aquifer (Hovorka and others, 2004; Worthington, 2004). The contribution of matrix permeability to regional-scale hydraulic conductivity likely is minor, and most Edwards aquifer water flows through fractures and conduits (Hovorka and others, 1998). Water entering the Edwards aquifer in the recharge zone moves downdip from unconfined to confined parts of the aquifer through generally southeasterly flow paths. In the confined zone of the San Antonio segment of the aquifer, the water moves under low hydraulic gradients through fractured, highly transmissive, cavernous strata toward the east and northeast, where it is discharged through springs (primarily Comal and San Marcos Springs) and high-capacity wells. In the Barton Springs segment of the aquifer, the ground-water-flow direction is generally to the east and northeast toward Barton Springs.

Faults can either increase or decrease total transmissivity in the Edwards aquifer (Hovorka and others, 1998) and thereby tend to convey or to restrict flow. Some of the abundant, interconnected fractures in intensely fractured and brecciated zones adjacent to faults have been enlarged, and they might focus flow parallel to faults. Where calcite cement fills breccia, cross-fault flow might be decreased. Stratigraphic offset of permeable zones along faults might also decrease the cross-fault flow (Maclay and Small, 1986). Maclay (1995) and Groschen (1996) characterized flow in the Edwards aquifer as being controlled laterally by barrier faults that locally compartmentalize, or restrict, flow within, to, and from parts of the aquifer, especially toward the eastern part of the San Antonio segment.

SIMULATION OF GROUND-WATER FLOW

A numerical model of ground-water flow was constructed on the basis of a conduit-flow dominated conceptual model of the Edwards aquifer. The FORTRAN computer-model code MODFLOW (McDonald and Harbaugh, 1988; Harbaugh and McDonald, 1996; Harbaugh and others, 2000), a modular finite-difference ground-water-flow code developed by the USGS, was used to simulate ground-water flow in the Edwards aquifer. As a way to represent conduits, other than by use of a coupled-continuum pipe flow or dual- or triple-porosity model, conduits are simulated in the Edwards aquifer model by narrow (one-cell wide), continuously connected zones with large hydraulic-conductivity values (fig. 2).

Calibration and evaluation of the Edwards aquifer model were conducted for steady-state (1939–46) and for transient (1947–2000) conditions. Once it was demonstrated that the model could approximate observed historical conditions (1947–90), the model then was used to simulate the effects of stresses for a time period not used initially for model calibration (model testing period, 1991–2000).

Model Description

The Edwards aquifer model area includes the San Antonio and Barton Springs segments of the Edwards aquifer. The model area was subdivided into rectangular finite-difference grid cells within which the properties of the aquifer material represented are assumed to be uniform. The uniformly

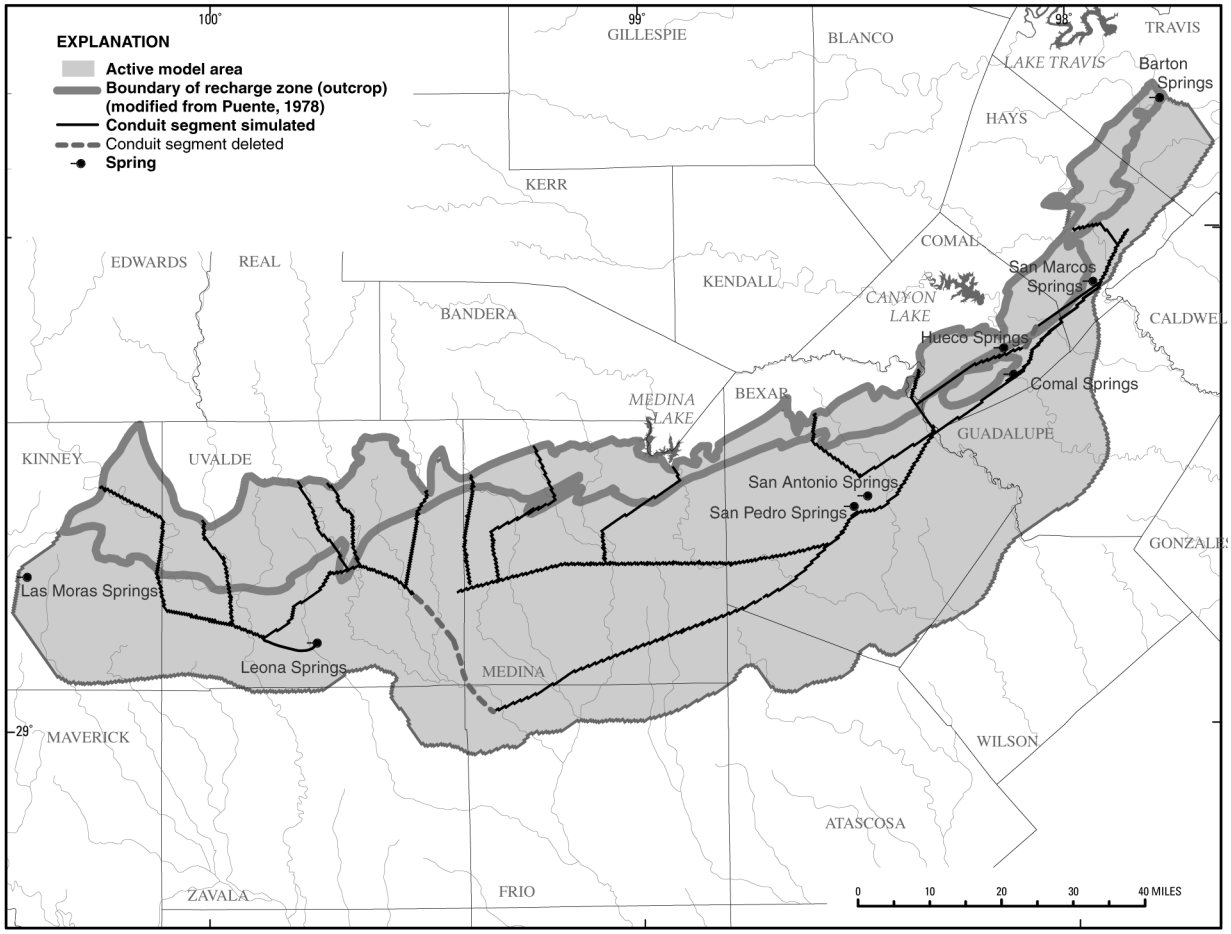

Figure 2. Simulated locations of conduits in the Edwards aquifer model, San Antonio region, Texas.

spaced finite-difference grid used to spatially discretize the model area has 370 rows and 700 columns. The dimensions of the grid cells are uniformly 0.25 mile (mi) (1,320 ft) along rows and columns, with about 33 percent of the cells in the grid being active. The grid was rotated 35 degrees counterclockwise from horizontal to achieve the best alignment with the direction of ground-water flow and orientation of major faults near Comal and San Marcos Springs. A single model layer was used to represent the multiple hydrogeologic units that comprise the Edwards aquifer. The Edwards aquifer was not discretized vertically because of a lack of sufficient hydrogeologic data needed to spatially define individual hydrogeologic units within the geologic section.

Where possible, natural hydrologic boundaries were used to establish the extent of the active area of the Edwards aquifer model. The northern boundary of the model corresponds to the northern limit of the Edwards aquifer recharge zone. A head-dependent flux boundary (MODFLOW general-head boundary package) was used for the northern model boundary to account for the inflow of water from the adjacent Trinity aquifer. During transient simulation, the MODFLOW well package was used to simulate a constant flux, equal to the model-computed general-head boundary flux of the steady-state simulation, through the northern model boundary for all stress periods.

The northern part of the eastern model boundary is defined by the location of the Colorado River, which is a regional sink for the Edwards aquifer. Stream-aquifer leakage is simulated in the model as head-dependent flux nodes using the MODFLOW river package (McDonald and Harbaugh, 1988). The southern part of the eastern model boundary (south of the Colorado River) was assigned a no-flow

boundary condition. The western model boundary coincides with the location of a poorly defined ground-water divide near Brackettville in Kinney County (LBG-Guyton Associates, 1995). Minimal flow across this boundary was assumed and a no-flow boundary condition was initially assigned. During model calibration, however, a specified-flux boundary, with inflow into the Edwards aquifer, was imposed for the northern part of the boundary. The southern part of the boundary was maintained as a no-flow boundary.

The southern Edwards aquifer boundary typically has been defined by the 1,000-milligrams per liter (mg/L) line of equal dissolved solids concentration, which coincides with the updip boundary of the transition zone (Schultz, 1993, 1994). The 10,000-mg/L concentration line (A.L. Schultz, consultant, written commun., 2000) was used in the Edwards aquifer model as a more conservative boundary, constituting the limit of ground-water flow in the freshwater zone of the aquifer. A no-flow boundary condition was imposed.

The anisotropic effects of faults were incorporated in the Edwards aquifer model using the MODFLOW horizontal-flow barrier package. The hydraulic characteristic of the barrier (fault) is an inverse measure of the degree to which it acts as a barrier to flow. The greater the assigned value for the hydraulic characteristic of the fault, the less it acts as a barrier to flow. For the model, the assumption was made that the degree to which a fault acts as a barrier to ground-water flow is proportional to the fault displacement, with the hydraulic characteristic of the barrier being inversely proportional to the fault displacement. The final calibrated hydraulic characteristic values assigned to simulated faults range from 1.0×10^{-9} to 2.0×10^{-2} $days^{-1}$.

The initial locations of conduit zones in the Edwards aquifer model were assigned on the basis of the conduit locations inferred by Worthington (2004, fig. 21). The confined-zone conduit segments are based on potentiometric-surface troughs, geologic structure, and preferential development of conduits near the freshwater/saline water transition zone. In addition, the major sinking streams were interpreted to be connected to the major springs by conduits. During model calibration, revisions were made to the simulated conduit segments, including the deletion of a northwest-southeast trending segment in southeastern Uvalde and northwestern Frio Counties (fig. 2).

The hydraulic-conductivity distribution for the Edwards aquifer model includes two components. The first component is the hydraulic-conductivity distribution developed by Painter and others (2002). An approach based on nonparametric geostatistics, stochastic simulation, and numerical flow simulation was used to upscale and interpolate hydraulic-conductivity estimates to the model grid. The second component, superimposed on the base distribution of Painter and others (2002), is the network of conduits, initially as inferred by Worthington (2004, fig. 21). For the Barton Springs segment of the aquifer, the hydraulic-conductivity distribution from Scanlon and others (2002), rather than that of Painter and others (2002), was used. Horizontal hydraulic conductivities were varied during model calibration to better match measured hydraulic heads and springflows. Hydraulic conductivities were decreased by varying amounts, as compared to the initial simulated values from Painter and others (2002), in Kinney County and south of the 1,000-mg/L dissolved solids concentration line.

Liedl and others (2003) and Worthington (2004) indicate that conduits increase in size or number, or both, in the direction of downgradient springs. Therefore, the final calibrated hydraulic conductivities assigned to the conduits were: (1) 1,000 to 10,000 ft/d for the conduit segments originating in the recharge zone, farthest from Comal and San Marcos Springs and areas of lesser conduit development (Hovorka and others, 1998; Worthington, 2004), (2) 100,000 ft/d for the segments in the confined zone of the aquifer, but still distant from the major springs, and (3) 200,000 ft/d for the segments in the confined zone of the aquifer near the major springs.

Storativity values, including specific storage and specific yield, were assigned to each active cell for the transient simulations. Initially, uniform values for specific storage and specific yield were assigned, on the basis of reported values from

previous numerical ground-water-flow models of the aquifer (Maclay and Land, 1988; Scanlon and others, 2002). Storativity values subsequently were varied during model calibration, resulting in a zonation of values. The final calibrated storativity zones include five zones for specific yield, ranging from 0.005 to 0.15, and five zones for specific storage, ranging from 5.0×10^{-7} to 5.0×10^{-6} ft^{-1}. The storativity values of the simulated conduit cells are the same as the values for the non-conduit cells in the storativity zone in which the conduit cells occur.

A specified-flux boundary, simulated using the MODFLOW recharge package, was used to represent recharge to the Edwards aquifer in the recharge zone (McDonald and Harbaugh, 1988). Simulated recharge to the aquifer by seepage from streams and infiltration of rainfall was assigned to cells in the recharge zone for eight major recharging streams and their interstream areas (recharge subzones), on the basis of annual recharge rates to the Edwards aquifer calculated by the USGS for 1934–2000. Average annual recharge rates during 1939–46 were applied for the steady-state simulation. Monthly recharge rates were applied for the transient simulation (1947-2000). The simulated annual and monthly recharge rates for six recharge basins in the Barton Springs segment of the aquifer were derived from published rates in Slade and others (1986) and unpublished rates compiled by B.R. Scanlon (University of Texas, Bureau of Economic Geology, written commun., 2001). For both the San Antonio and Barton Springs segments, 85 percent of the recharge was applied to streambed cells and the remaining 15 percent applied to the interstream cells. As a result of model calibration, the simulated recharge rates for periods of greatly above-normal rainfall and recharge were reduced, as compared to reported rates. The USGS reported monthly recharge rates for the years 1958, 1973, 1981, 1987, 1991, and 1992 were multiplied by factors ranging from 0.60 to 0.85. The reported annual recharge for each of these years was greater than 1,400,000 acre-ft. The USGS reported recharge rates for the Cibolo Creek and Dry Comal Creek recharge subzone were reduced by 50 percent for all stress periods.

The primary simulated discharges of water from the Edwards aquifer are withdrawals by wells and springflows. The MODFLOW well package was used to simulate the withdrawals by wells. As with recharge, average withdrawal rates during 1939–46 were used for steady-state simulations, and monthly rates were assigned for each stress period of the transient simulation. Comal, San Marcos, Leona, San Antonio, and San Pedro Springs were simulated in the Edwards aquifer model and used for model calibration. The springs were simulated in the model using the MODFLOW drain package.

Model Calibration

The steady-state calibration targets for the Edwards aquifer model include: (1) average measured water levels during 1939–46 in 144 wells and (2) median springflows during 1939–46 for Comal, San Marcos, Leona, San Antonio, and San Pedro Springs. The mean absolute difference between simulated and measured hydraulic heads is 19.4 ft, and the mean algebraic difference is 4.5 ft, indicating the positive differences were approximately balanced by the negative differences. The root mean square (RMS) error for the 144 target wells is 26.5 ft, representing about 4 percent of the total head difference across the model area. The closest-match simulated springflows were within 3 and 13 percent of the measured median springflows for Comal and San Marcos Springs, respectively.

The transient calibration targets include: (1) synoptic sets of water levels in multiple wells during periods of below-normal and above-normal rainfall (potentiometric surface maps), (2) a series of measurements of water level within single wells over time (hydrographs), and (3) springflows for 1947–2000 for Comal, San Marcos, Leona, San Antonio, and San Pedro Springs. The closest-match simulated hydraulic heads for the transient simulation for a period of below-normal rainfall (May–November 1956, during the 1950s drought, when the lowest water levels on record were recorded) were within 30 ft of measured water levels at 123 of the 172 wells for which water-level data were available. The RMS error is 58.7 ft, representing about 8 percent of the total head difference across the model area. The closest-match simulated hydraulic heads for a period of above-normal rainfall (November 1974–July 1975, a period of near record-high water levels in

wells) were within 30 ft of measured water levels at 129 of the 169 wells for which water-level data were available. The RMS error is 33.5 ft, representing about 5 percent of the total head difference across the model area.

The transient simulation for 1947–2000 acceptably reproduces measured fluctuations in hydraulic heads in the Edwards aquifer. The match between simulated and measured hydraulic heads is generally closer for wells completed in the confined zone of the aquifer than for those in and near the recharge zone. The RMS error ranged from 4.1 to 23.2 ft in 11 wells with water-level measurements for varying periods during 1947–2000; these errors represent 7.8 to 30.8 percent of the range in water-level fluctuations of each well.

Generally acceptable agreement also was obtained between simulated and measured springflow at the simulated springs. The RMS errors for Comal, San Marcos, Leona, San Antonio, and San Pedro Springs ranged from 230,700 cubic feet per day (ft^3/d) for San Pedro Springs to 3,967,000 ft^3/d for Comal Springs. The RMS errors for the five springs, as a percentage of the range of springflow fluctuations measured at the springs, varied from 7.0 percent for San Marcos Springs to 36.6 percent for Leona Springs and were less than 10 percent for all but Leona Springs. The mean algebraic differences between simulated and measured spring discharges are 6.7 and 15.0 ft^3/s for Comal and San Marcos Springs, respectively, indicating a small bias in the residuals toward high flows.

Model Results

A ground-water divide in the Edwards aquifer occurs near Kyle in south-central Hays County, from which ground-water flow is to the east toward Barton Springs or to the west toward San Marcos Springs. Model simulation results indicate that the position of this ground-water divide varies, depending on the water-level conditions. For steady-state and above-normal rainfall and recharge conditions, the simulated position of the ground-water divide is coincident with its commonly defined position near Kyle. In contrast, during drought conditions the position of the simulated ground-water divide shifts westward to near San Marcos Springs.

Simulation results indicate that the simulated flow in the Edwards aquifer model is strongly influenced by the locations of the simulated conduits, which tend to convey flow. The simulated subregional flow directions are generally toward the nearest conduit and subsequently along the conduits from the recharge zone into the confined zone and toward the major springs. The influence of simulated barrier faults on flow directions is most evident in northern Medina County. In this area, the direction of ground-water flow is affected primarily by parallel northeastward-striking faults and conduit segments that divert the flow toward the southwest.

For the steady-state simulation, recharge accounts for 93.5 percent of the sources of water to the Edwards aquifer, and inflow through the northern and northwestern model boundaries contributes 6.5 percent. The largest discharges are spring discharge (73.7 percent) and ground-water withdrawals by wells (25.7 percent). The principal source of water to the aquifer for the transient simulation is recharge. The principal discharges from the aquifer for the transient simulation are springflows and withdrawals by wells. During 1956, representing drought conditions, the change in storage (net water released from storage) is much greater than recharge, comprising 75.9 percent of the total flow compared to 14.5 percent for recharge. Conversely, during 1975, representing above-normal rainfall and recharge conditions, recharge constitutes 79.9 percent of the total flow compared to 7.1 percent for the change in storage (net water added to storage).

A series of sensitivity tests were made to ascertain how the model results were affected by variations greater than and less than the calibrated values of input data. Simulated hydraulic heads and spring discharge in the Edwards aquifer model were most sensitive to recharge, withdrawals, hydraulic conductivity of the conduit segments, and specific yield; and comparatively insensitive to spring-orifice conductance, northern boundary inflow, and specific storage. Larger values of hydraulic conductivity, coupled with reduced recharge because model cells went dry, resulted in smaller simulated springflows.

If the reduced recharge is accounted for, however, larger values of hydraulic conductivity result in increased springflows. The effect of lowering the simulated spring-orifice altitudes of Comal and San Marcos Springs was to appreciably lower simulated hydraulic heads in the aquifer, because the spring-orifice altitudes serve as a controlling base level for hydraulic heads in the aquifer. The effect on simulated springflow was to minimally increase springflow for Comal Springs and appreciably decrease springflow for Leona Springs.

REFERENCES

Atkinson, T.C., 1977, Diffuse flow and conduit flow in limestone terrain in the Mendip Hills, Somerset (Great Britain): Journal of Hydrology, v. 35, no. 1–2, p. 93-110.

Elliott, W.R., and Veni, George, eds., 1994, The caves and karst of Texas—Guidebook for the 1994 convention of the National Speleological Society with emphasis on the southwestern Edwards Plateau: Huntsville, Ala., National Speleological Society, 342 p.

Groschen, G.E., 1996, Hydrogeologic factors that affect the flowpath of water in selected zones of the Edwards aquifer, San Antonio region, Texas: U.S. Geological Survey, Water-Resources Investigations Report 96–4046, 73 p.

Hamilton, J.M., Johnson, S., Esquilin, R., Thompson, E.L., Luevano, G., Wiatrek, A., Mireles, J., Gloyd, T., Sterzenback, J., Hoyt, J.R., and Schindel, G., 2003, Edwards Aquifer Authority hydrogeological data report for 2002: San Antonio, Tex., Edwards Aquifer Authority, 134 p. [Available online at www.edwardsaquifer.org.]

Harbaugh, A.W., Banta, E.R., Hill, M.C., and McDonald, M.G., 2000, MODFLOW–2000, the U.S. Geological Survey modular ground-water model—User guide to modularization concepts and the ground-water flow process: U.S. Geological Survey Open-File Report 00-92, 121 p.

Harbaugh, A.W., and McDonald, M.G., 1996, User's documentation for MODFLOW–96, an update to the U.S. Geological Survey modular finite-difference ground-water flow model: U.S. Geological Survey Open-File Report 96–485, 56 p.

Hovorka, S.D, Mace, R.E., and Collins. E.W., 1998, Permeability structure of the Edwards aquifer, south Texas—Implications for aquifer management: Austin, University of Texas, Bureau of Economic Geology Report of Investigations 250, 55 p.

Hovorka, S.D., Phu, T, Nicot, J.P., and Lindley, A., 2004, Refining the conceptual model for flow in the Edwards aquifer—Characterizing the role of fractures and conduits in the Balcones fault zone segment: Contract report to Edwards Aquifer Authority, 53 p.

Johnson, S.B., Schindel, G.M., and Hoyt, J.R., 2002, Ground-water chemistry changes during a recharge event in the karstic Edwards aquifer, San Antonio, Texas: Geological Society of America, Online Abstract 186–8.

LBG-Guyton Associates, 1995, Edwards aquifer groundwater divides assessment, San Antonio region, Texas: San Antonio, Edwards Underground Water District Report 95–01, 35 p.

Liedl, R., Sauter, M., Hückinghaus, D., Clemens, T., and Teutsch, G., 2003, Simulation of the development of karst aquifers using a coupled continuum pipe flow model: Water Resources Research, v. 39, no. 3, p. 1,057–1,067.

Lindgren, R.J., Dutton, A.R., Hovorka, S.D., Worthington, S.R.H., and Painter, Scott, 2004, Conceptualization and simulation of the Edwards aquifer, San Antonio region, Texas: U.S. Geological Survey Scientific Investigations Report 2004–5277, 143 p.

Mace, R.E., Chowdhury, A.H., Anaya, Roberto, Way, S.C, 2000, Groundwater availability of the Trinity aquifer, Hill Country area, Texas—Numerical simulations through 2050, Texas Water Development Board Report 353, 169 p.

Maclay, R.W., 1995, Geology and hydrology of the Edwards aquifer in the San Antonio area, Texas: U.S. Geological Survey Water-Resources Investigations Report 95– 4186, 64 p.

Maclay, R.W., and Land, L.F., 1988, Simulation of flow in the Edwards aquifer, San Antonio Region, Texas, and refinements of storage and flow concepts: U.S. Geological Survey Water-Supply Paper 2336–A, 48 p.

Maclay, R.W., and Small, T.A., 1986, Carbonate geology and hydrology of the Edwards aquifer in the San Antonio area, Texas: Texas Water Development Board Report 296, 90 p.

McDonald, M.G., and Harbaugh, A.W., 1988, A modular three-dimensional finite-difference ground-water flow model: U.S. Geological Survey, Techniques of Water-Resources Investigations, book 6, chap. A1 [variously paged].

Ogden, A.E., Quick, R.A., Rothermel, S.R., and Lundsford, D.L., 1986, Hydrological and hydrochemical investigation of the Edwards aquifer in the San Marcos area, Hays County, Texas: San Marcos, Tex., Edwards Aquifer Research and Data Center, 364 p.

Painter, Scott, Jiang, Yefang, and Woodbury, Allan, 2002, Edwards aquifer parameter estimation project final report: Southwest Research Institute [variously paged].

Puente, Celso, 1978, Method of estimating natural recharge to the Edwards aquifer in the San Antonio area, Texas: U.S. Geological Survey Water-Resources Investigations Report 78–10, 34 p.

Scanlon, B.R., Mace, R.E., Smith, Brian, Hovorka, S. D., Dutton, A.R., and Reedy, R.C., 2002, Groundwater availability of the Barton Springs segment of the Edwards aquifer, Texas—Numerical simulations through 2050: Austin, University of Texas, Bureau of Economic Geology, final report prepared for Lower Colorado River Authority under contract no. UTA99–0, 36 p.

Schindel, G.M., Johnson, S.B., Worthington, S.R.H., Alexander, E.C., Jr., Alexander, Scott, and Schnitz, Lewis, 2002, Groundwater flow velocities for the deep artesian portion of the Edwards aquifer, near Comal Springs, Texas, *in* Annual Meeting of the Geological Society of America, Denver, Colo., October 27–30, 2002: Geological Society of America Abstracts with Programs, v. 34, no. 6, p. 347.

Schultz, A.L., 1993, Defining the Edwards aquifer freshwater/saline-water interface with geophysical logs and measured data (San Antonio to Kyle, Texas): San Antonio, Edwards Underground Water District Report 93–06, Texas, 81 p.

Schultz, A.L., 1994, 1994 review and update of the position of the Edwards aquifer freshwater/saline-water interface from Uvalde to Kyle, Texas: San Antonio, Edwards Underground Water District Report 94–05, 31 p.

Slade, R.M., Jr., Dorsey, M.E., and Stewart, S.L., 1986, Hydrology and water quality of the Edwards aquifer associated with Barton Springs in the Austin area, Texas: U.S. Geological Survey, Water-Resources Investigations Report 86–4036, 96 p.

Tomasko, David, Fisher, Ann-Marie, Williams, G.P, and Pentecost, E.D, 2001, A statistical study of the hydrologic characteristics of the Edwards aquifer: Chicago, Argonne National Labs, 38 p.

Veni, George, 1988, The caves of Bexar County (2d ed.): Austin, University of Texas, Texas Memorial Museum Speleological Monograph 2, 300 p.

Worthington, S.R.H., 2004, Conduits and turbulent flow in the Edwards aquifer: Worthington Groundwater, contract report to Edwards Aquifer Authority, San Antonio, Tex., 41 p.

The Role of MODFLOW in Numerical Modeling of Karst Flow Systems

By J.J. Quinn, D. Tomasko, and J.A. Kuiper
Environmental Assessment Division, Argonne National Laboratory, Argonne, IL 60439

ABSTRACT

Mixed-flow karst systems convey groundwater through a combination of conduit and diffuse flow. Building a conceptual model of the flow system is possible, but advancing to the next stage, a numerical model, poses difficulties because of the complexities inherent to karst flow. Yet a numerical model may be desired to test the conceptual model, quantify fluxes, and identify data gaps.

Approaches to modeling karst flow have included the equivalent porous medium approach, black box reproductions of input and spring discharge, very high hydraulic conductivity flowpaths, fracture network simulations, and open channel equivalents. These are discussed in greater detail in Quinn and Tomasko (2000). All of these methods have advantages and disadvantages relevant to a given modeling purpose.

Numerical models of karst flow systems have traditionally relied on high-permeability zones to handle the karstified portion of a carbonate system, and springs have been represented by a single model feature, such as a drain cell, at the spring location. This approach, however, ignores the bulk of the flow from the conduit system. The question remains whether numerical models, such as the U.S. Geological Survey's MODFLOW, are suitable for creating models of karst flow systems.

This study illustrates a method of numerical modeling that has performed well in two case studies, one in Missouri and one in Germany. In each case, the conduit system is inferred by a variety of indirect evidence and modeled using MODFLOW as a network of connected drains feeding each outflow spring.

INTRODUCTION

The modeling of groundwater flow in karst aquifer systems is difficult because of the complexities of conduit geometries and arrangement and the relationship between diffuse and conduit flow within the aquifer. From local to regional scale, models constructed in karst settings require assumptions regarding the flow regime, as well as supporting data, some of which may be unavailable.

Numerical modeling of karst flow has nonetheless been attempted with a variety of approaches in two- or three-dimensional models of local to regional scale. Finite element examples include Laroque et al. (1999, 2000), who modeled springs as constant head locations, and Gonzalez-Herrara et al. (2002), who modeled karst features in a regional study area using equivalent porous media and large element dimensions. Examples of MODFLOW used in porous media are also in the literature (e.g. Witkowski et al. 2003, Guvanasen et al. 2000, Scanlon et al. 2003, Zhang and Keeler 1998, Langevin 2003, and Sepulveda 2002). Several of these papers are cases in which each spring was simulated as a single model cell with a MODFLOW drain (Scanlon et al. 2003, Sepulveda 2003) or with a MODFLOW general head boundary (Zhang and Keeler 1998). The approach of equivalent porous media with a single model feature representing each spring is limiting and generally restricted to regional water resources studies, and is not useful for local issues such as flow directions, flow rates, protection zone delineation, or point source contamination modeling (Scanlon et al. 2003, Langevin 2003).

APPROACH

In several examples discussed above, conduit flow was modeled by installing a drain or general head feature at a spring location. Calibration was achieved by adjusting hydraulic conductivity in a zone upgradient from the spring. However, this

technique ignores the rapid discharge to a conduit system laced throughout large portions of the aquifer.

Our approach relies on a conceptually more complete modeling of the inferred or estimated conduits. They are modeled as continuous, branching networks of MODFLOW drain cells. In this manner, diffuse discharge throughout the aquifer has the potential to reach tributaries of the conduit system, to be essentially removed from the flow system, and to be accounted for as discharge at the outlet spring in combination with all contributing conduit branches.

The MODFLOW drain package was originally developed to simulate drain tiles; however, it is a reasonable analogue for conduits in karst. Two types of information are needed as drain input. Drain elevations must be specified along a modeled conduit. At the downgradient end, these are set to the elevation of discharge spring, while at the upgradient locations, the elevations are specified based on drilling data. The second type of input is drain conductance. Setting this term to a high value promotes removal of water from flow system, and the model is insensitive to changes in its value.

This approach is geared toward solving a mixed-flow karst system, with equipotentials within the diffuse portion of the aquifer matrix bending at conduits (e.g., Field 1993, Quinlan and Ewers 1985).

The Groundwater Modeling System (GMS) is used as a pre- and post-processor. GMS assigns elevations along the drain segments by performing linear interpolation between the nodes of a branching system of drains.

Model calibration is made by manually adjusting elevations of drains, hydraulic conductivity, and recharge to match target heads and fluxes (spring outflow), or by parameter estimation of aquifer and recharge parameters.

SOURCES OF INPUT

Critical to implementing this approach is estimating or inferring the locations of conduits within the karst terrain. Drain networks were assigned in each study area by relying on available data, which could include dye tracing results, geophysical anomalies (lineaments), surficial features (dry valleys, fractures, sinkholes), spring locations, and spring flow measurements.

For assigning initial drain elevations, drilling data is used to estimate the depth of the weathered/unweathered contact within the carbonate. Initial values of hydraulic conductivity are assigned to zones on the basis of aquifer testing data.

MISSOURI CASE STUDY

This site, located on the Burlington-Keokuk limestone of Missouri, has input data in the form of numerous dye traces conducted by the Missouri DNR (Figure 1), a main spring with a long outflow monitoring record, abundant aquifer test data (Figure 2), widespread drilling data to determine the depth of the weathered zone, many monitoring wells for calibrating heads (Figure 3), and infiltration field studies to address specific site features. On the basis of drilling data and aquifer testing, the modeling included two layers: a deeper unweathered unit and a shallower weathered unit.

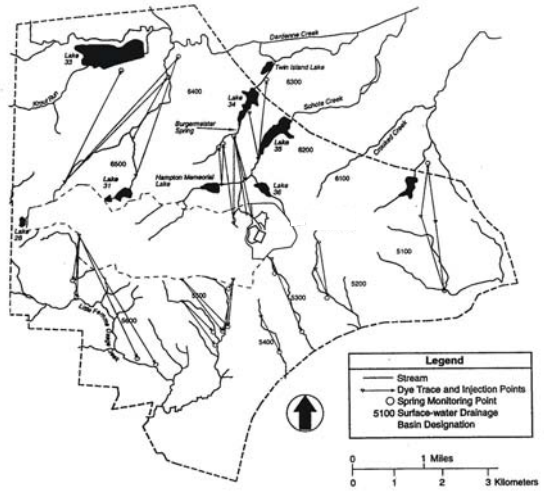

Figure 1. Site setting and results of Missouri DNR tests.

Calibration to the target head surface and to average flux at the main spring to the north was made by adjusting drain elevations. The resulting calibrated model (Figure 4) provided a strong match

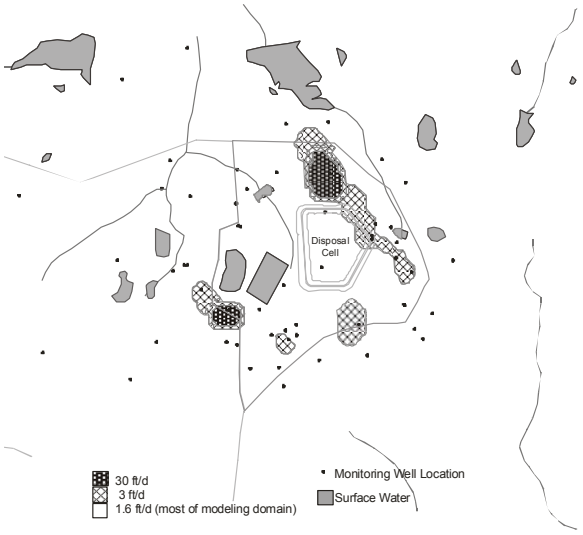

Figure 2. Hydraulic conductivity distribution of upper model layer, based on aquifer testing.

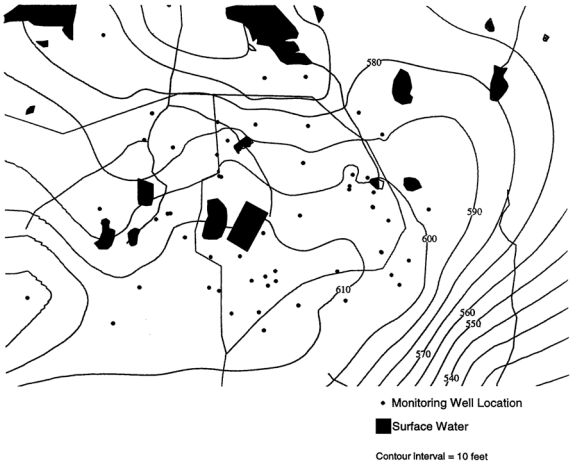

Figure 3. Target heads and monitoring well locations.

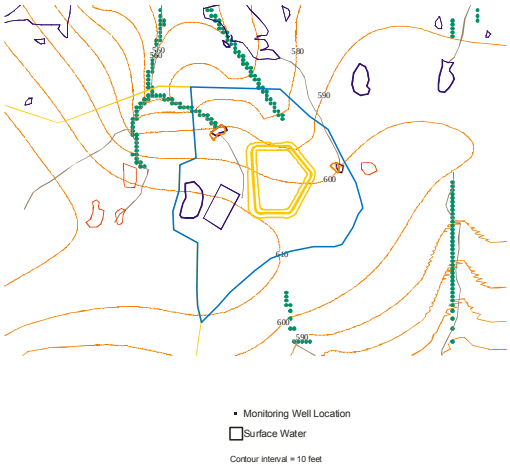

Figure 4. Missouri site calibrated heads.

to target heads and to spring outflow. Details of this study are provided in Quinn and Tomasko (2000). The flow model was used in an application to determine the effect a disposal cell would have on the local flow system.

GERMANY CASE STUDY

This site is the Hohenfels Combat Maneuver Training Center (CMTC), located on the Malm Formation of Bavaria (Figure 5). Portions of the study area have been intensively investigated by geophysicists of Argonne National Laboratory's Energy Systems Division. Their results identified numerous anomalies attributed to the presence of karst conduits (Figure 6). The site is primarily comprised of carbonates of the Malm Formation.

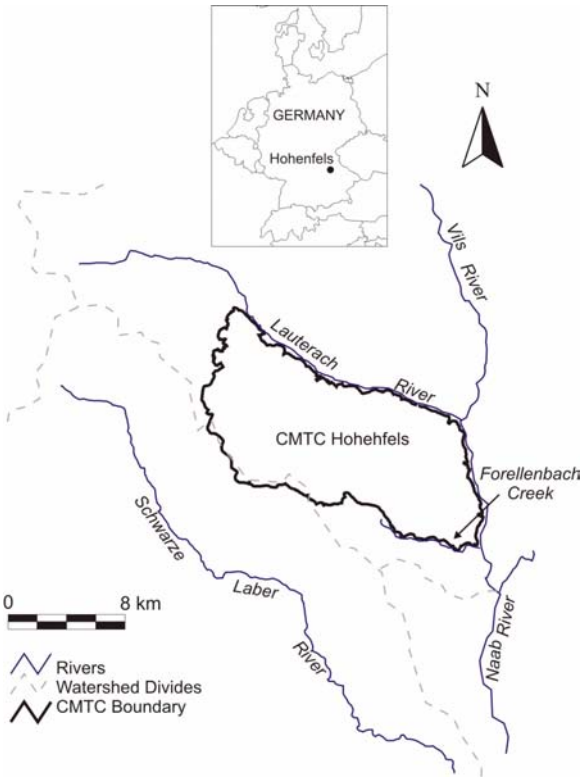

Figure 5. CMTC, Lautertal, and regional features.

The site characterization also includes several dye tracing experiments (Figure 7), limited coverage of monitoring wells and target head data, several measurements of spring flow, and detailed physical feature mapping (sinkholes, dry valleys) only on the training center property. The MODFLOW model of

this site included the entire CMTC site and extended to several external areas to make use of regional groundwater divides as boundary conditions. Drains were included in the finite-difference model on the basis of the dye traces, geophysical lineaments, and valley orientations.

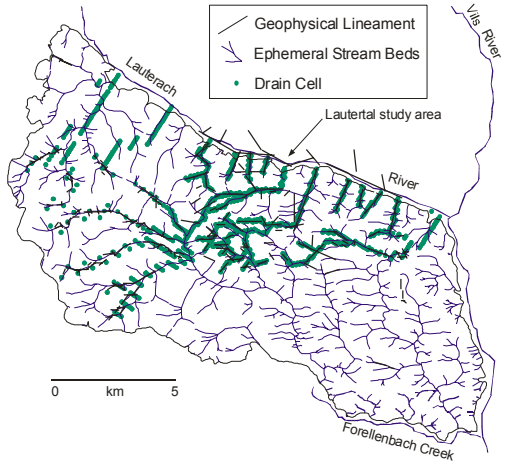

Figure 6. Drain cells and geophysical lineaments.

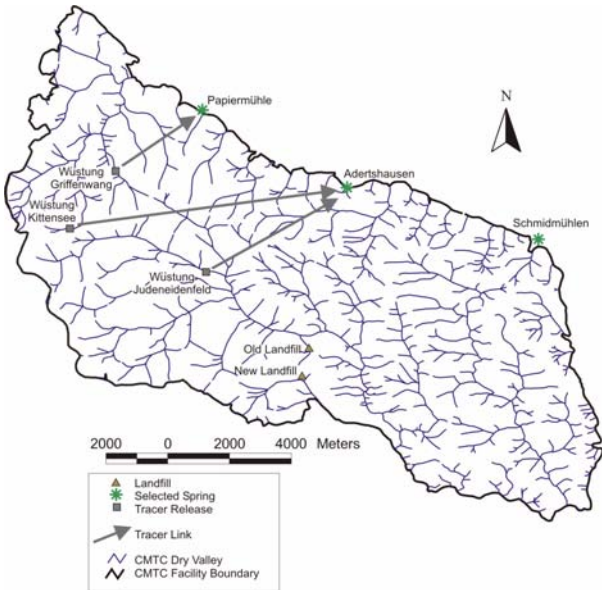

Figure 7. Hydraulic connections established through dye tracing.

The focus of the field and modeling efforts was a portion of the CMTC called the Lautertal. Here, model results clearly show the influence of the interconnected drain cells laced through the aquifer (Figure 8). Because of the sparse amount of target head data at the site, detailed calibration was not possible. However, the resulting heads of the calibrated model provide an adequate match to the available data in the area most intensively characterized with physical features mapping, geophysics, and tracer tests. Drain output matched reasonably well with spot measurements of outflow at several springs. Details of this study are provided in Quinn and Tomasko (2000) and Quinn et al. (in review).

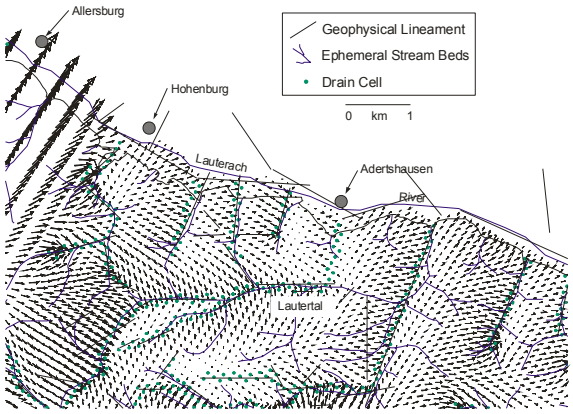

Figure 8. Zoom view of flow vectors near Lautertal, illustrating the relationship between the drain locations and the flow field.

CONCLUSIONS

Results from applying the technique of interconnected MODFLOW drain cells have shown promise in two case studies in mixed-flow karst terrain. Calibration to both target heads and target spring fluxes is achievable, though the calibration of transient models to varying spring discharge has not yet been attempted.

This approach is more realistic compared to other numerical approaches and has served well to test conceptual models and identify data gaps at two sites. It is also easy to implement with currently available software. The accuracy of the method depends on the coverage of quality field data, especially dye tracing, geophysics, hydraulic conductivity estimates, and target heads and fluxes (spring outflow). An advantage of this method is that the modeling is performed without detailed information on the geometry of the conduits, which is difficult or impossible to obtain.

REFERENCES

Field, M.S., 1993. Karst hydrology and chemical contamination. Journal of Environmental Systems, 22 (1), 1-26.

Gonzalez-Herrara, R., Sanchez-y-Pinto, I., and Gamboa-Vargas, J., 2002, Groundwater-flow modeling in the Yucatan karstic aquifer, Mexico: Hydrogeology Journal, vol. 10, p. 539-552.

Guvanasen, V., Wade, S.C., and Barcelo, M.D., 2000, Simulation of Regional Ground Water Flow and Salt Water Intrusion in Hernando County, Florida: Ground Water, vol. 38, no. 5, p. 772-783.

Langevin, C.D., 2003, Simulation of submarine ground water discharge to a marine estuary: Biscayne Bay, Florida: Ground Water, vol. 41, no. 6, p. 758-771.

Larocque, M., Banton, O., and Razack, M., 2000, Transient-State History Matching of a Karst Aquifer Ground Water Flow Model: Ground Water, vol. 38, no. 6, p. 939-946.

Larocque, M., Banton, O., Ackerer , P., and Razack, M., 1999, Determining karst tranmissivities with inverse modeling and an equivalent porous media: Ground Water, vol. 37, no. 6, p. 897-903.

Quinlan, J.F. and Ewers, R.O., 1985. Ground water flow in limestone terraces: strategy, rationale and procedure for reliable, efficient monitoring of ground water quality in karst areas. In: Proceedings, Fifth National Symposium on Aquifer Restoration and Ground Water Monitoring. National Water Well Association, Dublin, Ohio, pp. 197-234.

Quinn, J. and Tomasko, D., 2000, A Numerical Approach to Simulating Mixed Flow in Karst Aquifers, *in* I. Sasowsky and C. Wicks, eds., Groundwater Flow and Contaminant Transport in Carbonate Aquifers: Rotterdam, Holland, A.A. Balkema, p. 147-156.

Quinn, J.J., Tomasko, D., and Kuiper, J.A., in review, Modeling Complex Flow in a Karst Aquifer: submitted to Sedimentary Geology.

Scanlon, B.R., Mace, R.E., Barrett, M.E., and Smith, B., 2003, Can we simulate regional groundwater flow in a karst system using equivalent porous media models: Case study, Barton Springs Edwards aquifer, USA: Journal of Hydrology, vol. 276, p. 137-158.

Sepulveda, N., 2002, Simulation of ground-water flow in the Intermediate and Floridan Aquifer Systems in Peninsular Florida: U.S. Geological Survey, Water-Resources Investigations Report 02-4009.

Witkowski, A.J., Rubin, K., Kowalczyk, A., Rozkowski, A., and Wrobel, J., 2003, Groundwater vulnerability map of the Chrzanow karst-fissured Triassic aquifer (Poland): Environmental Geology, vol. 44, p. 59-67.

Zhang, Y.-K., and Keeler, R., 1998, Modeling of groundwater flow with MODFLOW in a fractured-karst aquifer in the Big Spring Basin, Iowa: Proceedings of MODFLOW `98: Golden, CO, International Ground Water Modeling Center, p. 149-156.

The Case of the Underground Passage: Putting the Clues Together to Understand Karst Processes

By B. Mahler[1], B. Garner[1], and N. Massei[2]
[1]U.S. Geological Survey, 8027 Exchange Drive, Austin, TX 78754
[2]UMR 6143 M2C, Département de Géologie, Université de Rouen, 76821 Mont Saint-Aignan cedex, France

ABSTRACT

Contaminants in surface water entering karst aquifers in focused recharge can be transported rapidly through the system to discharge at springs. Such contaminants act as anthropogenic tracers of ground-water transport; analysis of their breakthrough curves as they discharge from springs allows identification and apportionment of contaminant sources, and can provide insight into aquifer structure and function. At Barton Springs, the principal outlet for the Barton Springs segment of the Edwards aquifer, near Austin, Texas, breakthrough curves for several anthropogenic and natural tracers have been analyzed. The proportion of discharge composed of recent recharge is determined with a mixing model for oxygen-18: following rainfall, an initial increase in discharge related to pressure transfer is clearly seen, followed by a further increase consisting of an increasing proportion of recently recharged water, which reaches a maximum about 48 hours after rainfall. First appearance of contaminants varies from less than 20 to more than 40 hours after rainfall, depending on the contaminant, aquifer conditions, and location of contaminant source. Decomposition of breakthrough curves of sediment, nutrients, pesticides, and volatile organic compounds at the different spring orifices indicates the existence and approximate location of multiple conduit flow routes, contaminant times of travel, and probable contaminant sources. Differences in breakthrough curve shape and magnitude indicate urban runoff, contaminant spills, and infiltration through the soil zone as sources of different contaminants. Comparison of contaminant loads in recharging surface water to those estimated for the decomposed breakthrough curves allows apportionment of contaminants to the five watersheds contributing recharge to the aquifer.

Spatial and Temporal Variations in Epikarst Storage and Flow in South Central Kentucky's Pennyroyal Plateau Sinkhole Plain

By Chris Groves[1], Carl Bolster[2], and Joe Meiman[3]
[1]Hoffman Environmental Research Institute, Western Kentucky University, Bowling Green KY 42101
[2]USDA ARS Animal Waste Management Research Unit, Bowling Green KY 42104
[3]Division of Science and Resource Management, Mammoth Cave National Park, Mammoth Cave, KY 42259

ABSTRACT

The well-developed karst aquifers of south central Kentucky's Pennyroyal Plateau are impacted by contamination from animal waste and other agricultural inputs. Understanding fate and transport of these and other contaminants first requires knowledge of flow and storage behaviors within the impacted aquifers, complicated by significant heterogeneity, anisotropy, and rapid temporal variations. Here we report on spatial and temporal variations in vadose zone flow and water chemistry (or quality) within Cave Spring Caverns, Kentucky beneath agricultural lands on a well-developed sinkhole plain. Weekly sampling of three underground waterfalls show statistically significant differences in water quality, though the sites are laterally within 160 m and are all located about 25 m underground, in a groundwater basin of about 315 km^2. These reflect a combination of differences in epikarst flow and land use above the cave. High-resolution (minutes) monitoring of precipitation recharge along with flow and specific conductance in one of the waterfalls reveals a significant storage and mixing reservoir within the soil/epikarst zone. Varying precipitation rates and antecedent moisture conditions result in a range of storm responses observed at the waterfall, depending in part on whether this reservoir is filled or depleted. Slow and rapid flow paths through this storage zone were observed, the latter triggered by high recharge rates. These observations are generally consistent with the interpretations of Perrin and others (2003) from a Swiss limestone aquifer in a somewhat different hydrogeologic setting, strengthening the idea that epikarst and, more generally, vadose zone storage play a key role influencing flow and transport within karst aquifer systems.

INTRODUCTION

Well-developed karst aquifers are extremely vulnerable to contamination due to the ease and rapidity with which fluids can enter and move through these systems. For example, within south central Kentucky's Pennyroyal Plateau, contamination of groundwater by agricultural contaminants associated with animal waste such as fecal bacteria and nitrate is widespread (Currens, 2002; Conrad and others, 1999). Understanding agricultural impacts on karst aquifers is particularly challenging due to significant heterogeneity and anisotropy typically found in these systems, which can lead to large spatial and temporal variations in flow and water chemistry conditions.

The *epikarstic,* or *subcutaneous* zone (Williams, 1983; Perrin and others, 2003; Jones and others, 2003) forms an important component of many karst flow systems. The typically perched epikarst aquifer forms in the vicinity of the soil/bedrock interface where fractures have been widened from dissolution by acidic soil water. As the infiltrating water quickly approaches equilibrium with respect to the limestone bedrock, dissolution rates drop, as does solutionally-enhanced permeability. As a result the epikarst constitutes a relatively high permeability zone in comparison with less permeable rocks below. Evaluating the impacts of epikarst flow and storage is critical for understanding the fate and transport of agricultural contaminants within karst aquifers.

Recently progress has been made in understanding the details of karst flow and geochemical processes by high-resolution monitoring with electronic probes and digital data loggers (e.g. Baker and Brunsdon, 2003; Charleton, 2003; Groves and Meiman, 2005; Liu and others, 2004). The importance for understanding karst dynamics comes not as much for the ability to automatically collect data in relatively remote locations, as for the ability to collect high temporal resolution data. Flow and chemical data with a resolution of minutes capture all significant structures of hydrologic variation, even for karst systems. This can be useful for interpreting information about aquifer structure by comparing the detailed timing and magnitudes of related phenomena. In a recent example, Liu and others (2004) interpreted controls on aquifer behavior in southwest China's tower karst by comparing rates, directions, and magnitudes of changes in water levels, specific conductance (spC), saturation indices, and PCO_2 in storm responses from a large karst spring and nearby well.

While the long-term goal of the research we describe here is to quantitatively understand fundamental controls on relationships between agricultural land use and karst groundwater quality, here we evaluate epikarst flow and storage within south central Kentucky's Pennyroyal Plateau sinkhole plain based on vadose water sampling from three waterfalls located beneath active farming land. Evaluating the hydrologic behavior of the epikarst at the site is a critical step to quantitatively evaluating the fate and transport of agricultural contaminants.

FIELD SITE

Three subsurface waterfalls are being monitored, as well as rainfall and other atmospheric parameters, within and above Cave Spring Caverns (Figures 1-4) near Smiths Grove, Kentucky. The cave is located beneath a small portion of the extensive sinkhole plain of the Pennyroyal Plateau within the Mississippian Plateaus Section of the Interior Low Plateaus Physiographic Province. Just over 2 km of large horizontal cave passages pass beneath several farm fields, with the cave floor typically about 25 m below the ground surface. Water enters at numerous locations as perennial or intermittent streams or waterfalls. The recharge area lies within the Graham Springs Groundwater Basin (Ray and Currens, 1998) which discharges at Wilkins Bluehole on the Barren River, 18 km to the southwest. Wilkins Bluehole is the second largest spring in Kentucky, with a minimum discharge of 0.56 m^3/s (Ray and Blair, in press).

The cave is formed within the upper part of the Mississippian St. Louis Limestone (Richards, 1964). The Lost River Chert, a discontinuous unit of silica-replaced limestone typically 2-3 m thick near the site, lies between the ground surface and the cave. Locally, beds dip gently to the west at about 1-2º.

South central Kentucky has a humid-subtropical climate. Using climatic data from the Mammoth Cave and Bowling Green areas, Hess (1974) estimated that the area has a mean precipitation of 1,264 mm/yr, and the mean-annual temperature is 13ºC. Late summer and early fall are drier than other months. Hess (1974) estimated that mean-annual potential evaporation is 800 mm, varying from near zero to over 100 mm/mo.

The three percolation waterfalls--1, 2, and 3 in order moving into the cave--fall between about 5 and 8 m from the ceiling along the east side of the main passage starting about 40 m north of the cave's entrance, within a 160 m section of the passage (Figure 1).

METHODS

There are three related sampling programs: surface weather conditions, weekly sampling and laboratory analysis of water at the three waterfalls, and 2-minute monitoring of flow, specific conductance (spC), pH, and temperature at waterfall 1. Details of these sampling programs are provided as follows:

Surface Rainfall

On the surface 110 m south of the cave entrance is an automated HOBO™ weather station that collects rainfall, temperature, wind speed and direction,

relative humidity, and solar radiation (Figure 2). Rainfall is resolved to the nearest 0.25 mm, and summed every five minutes. Due to interference by birds over part of the reported period, we utilized five-minute rainfall after 25 March 2005 (including storms 2, 3, and 4 discussed below) from the National Park Service Atmospheric Monitoring Station near the town of Pig, 9.5 km to the northeast.

Field Collection and Laboratory Analysis

Water was collected from each waterfall weekly in sterile, acid-washed HDPE bottles and stored on ice. In most cases water was analyzed within three hours of collection. Water samples were analyzed for a suite of parameters indicative of limestone weathering (e.g. Ca, Mg, alkalinity, and specific conductance (spC)) and agricultural impact (e.g., NO_3, PO_4, and NH_4). Alkalinity was measured using the inflection point titration method (Rounds and Wilde, 2001) and reported as mg/L $CaCO_3$ mg/L. Ca and Mg were analyzed in triplicate using inductively coupled plasma optical emission spectroscopy (ICP-OES). NO_3, PO_4, and NH_4 were measured in triplicate using a Lachat "QuickChem" method. Preliminary analysis indicated that particulate-associated Ca, Mg, and nutrients were minimal; subsequently water samples were not filtered prior to analysis. Dissolved oxygen (DO), pH and spC were measured in the field with a YSI 556 multi probe system (YSI Environmental). Data were collected from February 23, 2005 to May 25, 2005 for Ca, Mg, spC, and DO (n=13), March 3, 2005 to May 25, 2005 for alkalinity (n=12), and March 23, 2005 to May 25, 2005 for NO_3, PO_4, and NH_4 (n=10).

Data Logging at Waterfall One

The site is equipped with an array of electronic sensors and loggers and tied to a common tipping bucket rain gauge (Campbell Scientific (CSI) TE525) resolving tips of 0.1 mm. Discharge from the rain gauge is directed into 10-mm Tygon tubing which feeds a PVC flow-through chamber (20 mm ID) mounted with a series of three Cole-Parmer double-junction industrial in-line ATC pH sensors. Each pH sensor is connected to a three-meter shielded coaxial cable and terminates in the instrument box (Pelican 1400) at a Cole-Parmer preamplifier to increase signal stability. This pH system can resolve pH to +/- 0.01 SU. The pH flow-through chamber discharges into a section of 10-mm Tygon tubing where it is split into three paths, each passing through a CSI CS547A-L specific conductance/temperature sensor. This sensor can resolve temperature to +/- 0.1^{o}C and specific conductivity to +/- 0.001 mS. The three paths are then rejoined into a single section of tubing and positioned at an elevation approximately 40 cm higher than the sensors to assure pipe-full conditions. The signal from the rain gauge is split into three cables, each connected to a CSI CR10X digital micrologger (Figure 3). Each micrologger is connected to its corresponding set of pH, conductivity (spC) and temperature sensors. This redundancy in spC, temperature, pH, and data loggers not only ensures backup in the case of malfunction, but when fully operational we calculate means, standard deviations, and coefficients of variation (CV) for each observation. The 14,359 spC observations (each made in triplicate) reported in this paper had an average CV of 2.7%. This value is similar to the CV of Waterworks Spring (2%) which has been considered the only perennial "diffuse flow" spring in the region. Waterworks Spring is located near conduit dominated Wilkins Bluehole, which has a greater CV at 14% (Quinlan and others, 1983; p. 57).

Every 30 seconds the micrologger program is executed. The program is set to output tip totals from the rain gauge every five minutes, and to average the 30-second pH, spC, and temperature values every two minutes. To reduce redundant data the program compares the current two-minute average values of each sensor to that of the previous two-minute average. If the absolute value of change exceeds a preset value--the current two-minute average values for all sensors is committed to final storage. In any event, the current two-minute values are always stored once per hour. In this way we achieve two-minute resolution even during hourly recording, because we know under those static conditions the observations have not varied beyond the threshold value.

The waterfall flow data are given in tips per minute for the tipping bucket gage, but these do not yield discharge directly because some of the water, especially at higher flows, falls outside of the bucket orifice. These data thus only give a relative flow indication, but the signals (Figure 5) give a clear indication of dry and wet conditions and their correlation with rainfall events. We are in the process of developing a rating curve relating tips per minute to actual discharge, which we measure periodically by catching the flow in a large tarp and measuring the volumetric flow rate with a 10 liter bucket.

Statistical Analysis of Water Quality Data

Single-factor analysis of variance (ANOVA) was used to determine if statistically significant differences exist in important water quality parameters between the three waterfalls. Differences between waterfall locations may reflect different residence times and land use activities at the surface. Prior to analysis, Ca, NO_3, PO_4, and spC were log-transformed whereas Mg was inverse-transformed to obtain approximately normal distributions. Alkalinity, on the other hand, was normally distributed so no transformation was needed. Fisher's t-test was used to compare means between different waterfalls (Helsel and Hirsch, 1993). All statistical analyses were performed using SAS version 9.1 (SAS Institute Inc., 2003).

RESULTS

Temporal Variations at Waterfall One

Between 21 March and 10 April 2005, precipitation, waterfall flow, and spC data reflect four succeeding rain events that occurred over progressively wetter antecedent moisture conditions. Although we currently lack data for a rating curve, discharge directly measured under very dry conditions at the waterfall (31 May 2005) was 0.04 L s^{-1}. Using an empirical value of 1.98 L s^{-1} km^{-2} for unit base flow (Quinlan and Ray, 1995), derived from preliminary data for the autogenic recharge area of the Graham Springs Basin (Joe Ray, Kentucky Division of Water, personal communication, 2005), this discharge corresponds to an estimated recharge area for the waterfall of about 2 ha. Estimates of three epikarst spring recharge areas at other sites in Kentucky range from 4-8 ha (Ray and Idstein, 2004). Although the rainfall data after 25 March (storms 2-4) are from 9.5 km away, they show close correlation to the cave signals when there was a response.

Responses of the cave parameters show a varying behavior following the different storm events and thus provide information on flow and storage within the aquifer system. Flow in the waterfall, initially under relatively dry conditions, began to increase within 2.3 hours of the onset of significant rainfall measured above the cave system, and showed a clear flow increase of about 120% that returned to the original condition within about 1.5 days. However, there was no systematic change in the spC signal following this rainfall, as explained later.

About three days later a more intense storm occurred with obvious differences in the cave response. While the timing of the flow increase was similar to the first storm (though rain data for this storm are from the NPS station), flow rates stayed more than twice as high as the initial condition for more than four days without significant rainfall, rather than returning quickly to pre-storm levels. The spC signal from relatively dilute rainfall quickly moving through the system was also clear and corresponded to rainfall intensity, reaching a low of about 160 μS cm^{-1}, or about 70% of pre-storm levels, after an intense thunderstorm cell in which rainfall intensity exceeded 5 cm hr^{-1}. We lost data on peak waterfall flow rate because the flow exceeded the limits of the tipping bucket mechanism, but later modified the equipment to accommodate higher flows.

The next storm, about four days later, was different from the first two with respect to both signals. Flow rates continued at a similarly high level without an appreciable increase, while spC dropped again in very clear relation to rainfall. In contrast to the second storm, however, spC took more than seven days to rise to the same level that had taken

only two days after the previous rainfall, even though starting at a higher minimum level.

Finally, a small storm about five days later, which began with waterfall flow rates at a similarly high rate and spC still uniformly rising through time to pre-storm three levels, had little or no impact on waterfall behavior.

Spatial Water Quality Variations

Significant variations in water quality were observed between the three waterfalls (Figure 6). Both Ca and Mg were significantly higher in waterfall 2 and this is consistent with higher alkalinity and spC values at this location. The average Ca concentration for waterfall 2 was 50.7 mg L^{-1} compared to 32.1 mg L^{-1} and 33.4 mg L^{-1} for waterfalls 1 and 3, respectively (Figure 6A). Similarly, the average concentration of Mg in waterfall 2 was 8.57 mg L^{-1} compared to 5.93 mg L^{-1} for waterfall 1 and 5.02 mg L^{-1} for waterfall 3 (Figure 6B). Alkalinity and spC were also highest in waterfall 2. Mean alkalinity for waterfall 2 was 106 mg $CaCO_3$ L^{-1} and for waterfalls 1 and 3 the mean concentrations were 73.3 mg $CaCO_3$ L^{-1} and 60.0 mg $CaCO_3$ L^{-1}, respectively (Figure 6C). Mean spC was 328 μs cm^{-1} for waterfall 2, 236 μs cm^{-1} for waterfall 1, and 238 μs cm^{-1} for waterfall 3. Differences between waterfall 2 and waterfalls 1 and 3 were statistically significant at the 99% confidence level (Figure 6D).

As was the case with Ca, Mg, spC, and alkalinity, PO_4 was significantly higher in waterfall 2 ($p < 0.001$) compared to waterfalls 1 and 3 (Figure 6E). PO_4 concentrations averaged 0.204 mg L^{-1} in waterfall 2 whereas mean concentrations were only 0.063 mg L^{-1} and 0.047 mg L^{-1} for waterfalls 1 and 3, respectively. NO_3, on the other hand, was highest in waterfall 3 and lowest in waterfall 1 (Figure 6F). The average concentrations of NO_3-N were 10.4 mg L^{-1}, 8.19 mg L^{-1}, and 5.60 mg L^{-1} for waterfalls 1, 2, and 3, respectively. (For reference, the EPA NO_3-N Maximum Contaminant Level for drinking water is 10 mg L^{-1}) Statistical analysis on log-transformed NO_3-N data indicated that concentrations between the three waterfalls were significantly different ($p < 0.001$). NH_4 concentrations were at or below detection limit (0.02 mg L^{-1}) for all sampling times at each location.

DISCUSSION

Although the three waterfalls are separated laterally by a total of only about 160 m and at about the same depth underground, within a groundwater basin of over 315 km^2 (Ray and Currens, 1998), statistically significant differences occur in water chemistry between the three sites. These appear to result from a combination of different land use types and subsurface flow path conditions. Differences between parameters expected to result from dissolution of limestone, including Ca, Mg, alkalinity (closely related to bicarbonate concentrations), and spC, appear to indicate a difference in residence times for the flow paths leading to these waterfalls. Increased residence times may be due to greater flow path lengths and/or slower rates of movement through the epikarst and sections of the vadose zone below. Waterfall 2, for example (Figures 6A-6D), shows significantly higher concentrations than waterfalls 1 and 3 with respect to each of these four parameters.

The elevated concentrations of NO_3 and PO_4 measured in the waterfalls, particularly in waterfalls 2 and 3, suggest impact from agricultural land use in the cave's recharge zone. Although we currently lack data to discriminate the individual waterfall recharge zones (tracer testing is in progress to evaluate these), there are three different patterns in the concentrations of these compounds (Figures 6E and 6F) and indeed three general types of land use above the cave (Figure 1). Above and south of the first 90 m of the cave entrance (Figure 1, parcel A) is residential, the area to the north over the next 200 m (parcel B) had row crops (wheat) during the sampling period, and the area across the road to the east (parcel C) had cattle production. The row crops had both animal waste and chemical fertilizers applied before and during the study, while no chemicals were applied to either parcel A or C during or before sampling. While somewhat speculative until more data become available, a hypothesis consistent with the results so far might indicate that waterfalls 1, 2,

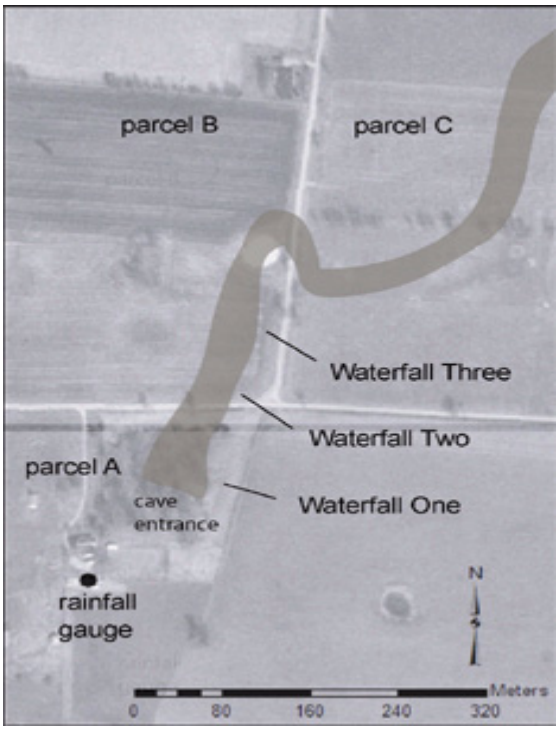

Figure 1. Map of the entrance area to Cave Spring Caverns showing sampling locations in relation to surface.

Figure 2. Weather station for recharge measurements, showing typical surface landscape above the cave system.

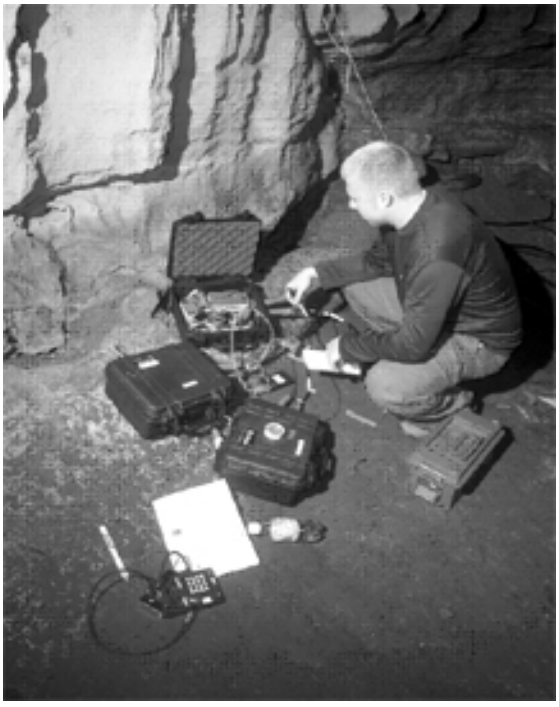

Figure 3. Triplicate Data logger system at Waterfall One.

Figure 4. Water sampling at Waterfall Three using remote device to avoid a shower while sampling.

and 3 have at least partial recharge zones in parcels A, B, and C, respectively. This is indicated by water relatively low in both NO_3 and PO_4 from A (residential), higher in both from B (animal and chemical fertilizers), and from C where NO_3 is high from cattle waste but PO_4 is low because no fertilizer was applied. As the rocks within which the cave has formed are dipping to the west, it is feasible that some parts of the waterfall recharge zones could be located to the east in parcel C.

Comparison between rainfall and flow and spC at waterfall 1 (Figure 6) reveals significant storage within the soil/epikarst above the cave, as well as slow and rapid flow paths through the epikarst whose functions depend on recharge rates and antecedent moisture. The spC signal at the onset of the record (~220 mS cm^{-1}) represents water that has reached an approximate chemical equilibrium with the soil/epikarst system. This signal is at times diluted by rainfall that has a typical spC of 10-15 mS cm^{-1} as measured at the NPS Atmospheric Monitoring Station (Bob Carson, National Park Service, personal communication).

While the flow conditions clearly responded to the input from the first rainfall (~day 81) the fact that spC did not change suggests that no dilute rainwater reached the probes, and that the storm input altered the hydraulic gradients within the epikarst in a way that pushed through a slug of previously-stored water, which drained through in about 1.5 days. While another possibility is that rainwater did indeed come through quickly but had within a short period developed the chemical characteristics of the epikarst storage, consideration of later storms, discussed below, makes this unlikely.

The intense rainfall beginning on day 86 was sufficient to impact the waterfall's spC indicating a relatively rapid transport of rainwater through the system within about one-half day, although it is impossible to measure this timing more accurately as these rainfall data came from 9.5 km away. Once this flow had been established, water from a large, very intense thunderstorm cell (occurring over the cave at about the same time as the more distant rain gauge, based on observations at the cave) caused a precipitous drop in spC within hours. While the spC returned to within 5% of its pre-storm values with less than eight hours after the spC minimum, the fact that flow remained high instead points to a significant epikarst storage reservoir. We interpret the differences in these two storms to suggest that this reservoir was relatively depleted during the dry antecedent conditions prior to the first storm, but was "replenished" during the large recharge event of storm 2. Differences in the three-dimensional head distributions within the epikarst water between the filled and depleted reservoir conditions account for differences in the responses. The more gradual return to prestorm spC conditions over the next several days reflects both mixing of storage and rainfall waters, as well as chemical reactions (limestone dissolution, for example) that increase the ionic strength of recharge water. The storm 2 response also suggests a recharge intensity threshold above which a rapid flow path is established, in addition to the more diffuse flow paths continually present.

These interpretations are consistent with the response from the third storm (day 92), which was intense but occurred under antecedent conditions with relatively full epikarst storage. The return to pre-storm chemical conditions is more gradual than in the previous storm, however, reflecting the greater proportion of storm to chemically equilibrated water within the reservoir. These two responses also indicate that the timescale for chemical mixing/ equilibration for these waters is on the order of several or more days, confirming that the slug of water pushed through during the first storm was already in the aquifer prior to that storm's onset.

Using flow and isotope measurements of rainfall and spring water, as well as underground streams leading to the spring, Perrin and others (2003) concluded that the soil/epikarst system forms an important mixing reservoir and were able to discriminate waters contributed by diffuse and rapid flow through the epikarst reservoir, the latter operating when a threshold recharge rate has been exceeded. These findings are similar to those obtained in the present study, and taken together, the

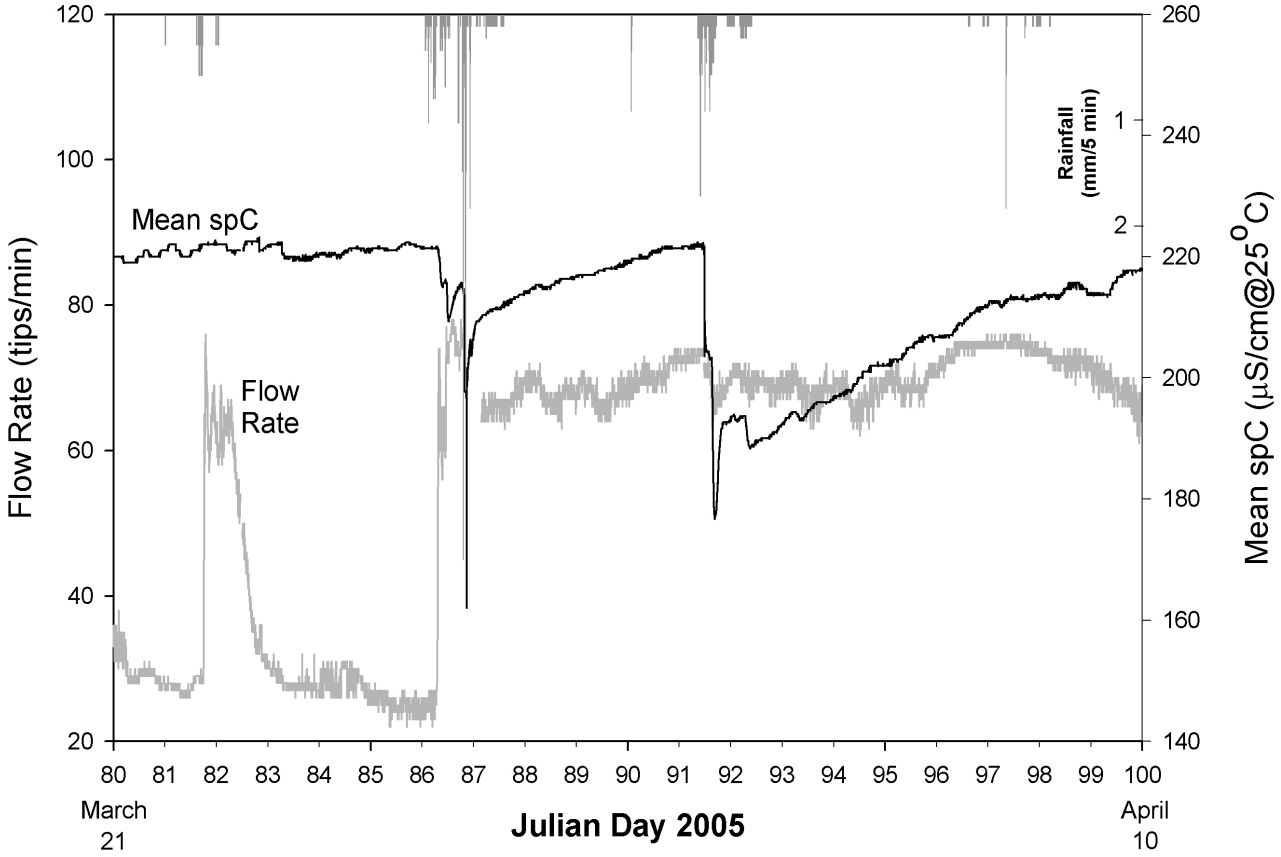

Figure 5. Plots of flow rate and mean specific conductance for waterfall 1 in Cave Spring Caverns, along with rainfall above the cave.

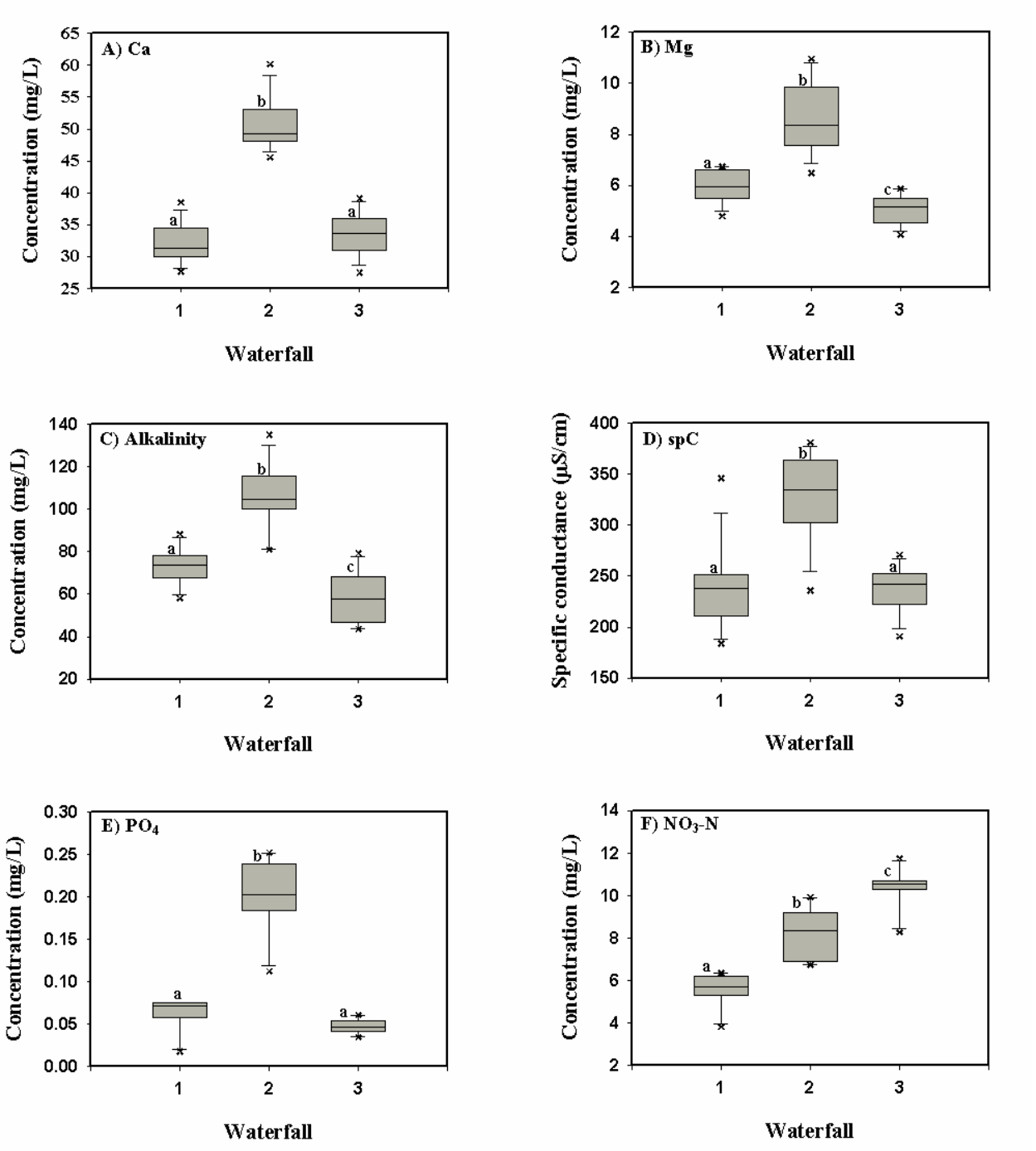

Figure 6. Boxplots of (A) calcium (mg L^{-1}), (B) magnesium (mg L^{-1}), (C) alkalinity as $CaCO_3$ (mg L^{-1}), (D) specific conductance (µS cm^{-1}), (E) phosphate (mg L^{-1}), and (F) nitrate-N (mg L^{-1}). boxes with same letter are not significantly different based on fisher's t-test on means of transformed (ca, Mg, Spc, NO_3, and PO_4) and untransformed ddata (alkalinity).

two studies provide quantitative evidence to strengthen the hypothesis that vadose zone storage plays a key role influencing flow and transport within a variety of karst aquifer systems.

ACKNOWLEDGMENTS

Funding for this work was provided by the US Department of Agriculture Agricultural Research Service. We appreciate very much the kind cooperation of Bill, Linda, and Nick Marohnic for access to their land and cave, as well as the assistance of Stacy Antle, Ben Estes, Deana Groves, Pat Kambesis, Tinesha Mack, Alanna Storey, Ben Tobin, Heather Veerkamp, and Carol Wicks who provided support to the project. We also thank Joe Ray and Chuck Taylor for thoughtful reviews of this manuscript.

REFERENCES

Baker, A. and C. Brunsdon, 2003, Non-linearities in drip water hydrology; an example from stump Cross Caverns, Yorkshire. *Journal of Hydrology,* v. 277, pp.151-163.

Charleton, R.A., 2003, Towards defining a scallop dominant discharge for vadose conduits; some preliminary results. *Cave and Karst Science*. v. 30, p. 3-7.

Conrad, P.G., D.I. Carey, J.S. Webb, J.S. Dinger, and M.J. McCourt, 1999, *Ground Water Quality in Kentucky: Nitrate-Nitrogen.* Kentucky Geological Survey Information Circular 60, Series IX, 5 p.

Currens, J.C, 2002, Changes in groundwater quality in a conduit-flow-dominated karst aquifer, following BMP implementation. *Environmental Geology*, v. 42, p. 525-531.

Groves, C. and J. Meiman, 2005, Weathering, geomorphic work, and karst landscape evolution in the Cave City groundwater basin, Mammoth Cave, Kentucky. *Geomorphology*, v. 67, p. 115-126.

Helsel, D.R., and R.M. Hirsch, 1993, Statistical methods in water resources. Elsevier, Amsterdam, p. 529.

Hess, J., 1974, *Hydrochemical Investigations of the central Kentucky Karst Aquifer System*. Ph.D. thesis, Department of Geosciences, The Pennsylvania State University.

Jones, W.K., D.C. Culver, and J.S. Herman (eds.), 2004, *Epikarst*. Charles Town, WV: Karst Waters Institute, 160 p.

Liu, Z., C. Groves, D. Yuan, and J. Meiman, 2004, South China Karst Aquifer Storm-Scale Hydrochemistry, *Ground Water***,** v. 42, p. 491-499.

Quinlan, J.F. and Ray, J.A., 1995, Normalized base-flow discharge of ground water basins: A useful parameter for estimating recharge area of springs and for recognizing drainage anomalies in karst terranes, *in* Beck, B.F. and Stephenson, B.F., ed., *The Engineering Geology and Hydrogeology of Karst Terranes*: Rotterdam, A.A. Balkema, p. 149-164.

Perrin, J., P-Y. Jeannin, and F. Zwahlen, 2003, Epikarst storage in a karst aquifer: a conceptual model based on isotopic data, Milandre test site, Switzerland. Journal of Hydrology vol. 279, p. 106–124.

Ray, J.A., and Idstein, P.J, 2004, Unpredictable surface exposure of epikarst springs in Kentucky, USA: *in* Epikarst, Jones, W.K., D.C. Culver, and J.S. Herman (eds.), Karst Waters Institute Special Publication 9, p. 140-141.

Ray, J.A. and Currens, J.C., 1998, Mapped karst groundwater basins in the Beaver Dam 30 x 60 Minute Quadrangle, Kentucky Geological Survey.

Richards, P.W., 1964, Geologic map of the Smiths Grove quadrangle, Kentucky. US Geological Survey Geologic Quadrangle Map GQ 357.

Rounds, S.A., and Wilde, F.D., eds., September 2001, Alkalinity and acid neutralizing capacity (2d ed.): U.S. Geological Survey Techniques of Water-Resources Investigations, book 9, chap. A6., section 6.6.

SAS System for Windows, version 9.1, SAS Institute Inc., Cary, NC, 2002.

Williams, P.W., 1983, The role of the subcutaneous zone in karst hydrology. *Journal of Hydrology* v. 61, p. 45-67.

Comparison of Water Chemistry in Spring and Well Samples from Selected Carbonate Aquifers in the United States

By Marian P. Berndt[1], Brian G. Katz[1], Bruce D. Lindsey[2], Ann F. Ardis[3], and Kenneth A. Skach[4]
[1]U.S. Geological Survey, 2010 Levy Avenue, Tallahassee, FL 32310
[2]U.S. Geological Survey, 215 Limekiln Road, New Cumberland, PA 17070
[3]U.S. Geological Survey, 8027 Exchange Drive, Austin, TX 78754
[4]U.S. Geological Survey, 10615 SE Cherry Blossom Drive, Portland, OR 97216

ABSTRACT

Water chemistry in samples from 226 wells and 176 springs were assessed to determine if samples from springs and wells have similar concentrations of selected properties such as dissolved solids, dissolved oxygen, nitrate, and calcite and dolomite saturation indices. Samples were collected in seven carbonate aquifers–Edwards-Trinity, Floridan, Mississippian, Basin and Range, Valley and Ridge, Springfield Plateau, and Ozark. Comparisons were made between concentrations of inorganic constituents in water samples from springs and from wells within the same aquifer. Results were variable, but showed that concentrations were not significantly different between samples from springs and wells for most properties. Nitrate and dissolved solids concentrations were only significantly different between spring and well samples in one or two of the seven aquifers; however, dissolved oxygen concentrations were significantly different between well and spring samples in four of the seven aquifers. Median calcite and dolomite saturation index values were significantly different between well and spring samples in three of the seven aquifers. Spring samples probably represent water from shallower parts of the aquifer flow systems and thus represent parts of the flow system that are most susceptible to contamination from land-use practices. These results indicate that the collection of water from springs should be considered critical to adequately characterize water quality in carbonate aquifers.

INTRODUCTION

About 20 percent of the ground water withdrawn for drinking water in the United States is from carbonate aquifer systems (M.A. Maupin, U.S. Geological Survey, written commun., 2004). Understanding the factors that control water quality in these systems requires information on water chemistry from the aquifer matrix, fractures, and from secondary porosity features (e.g., solution conduits). Com-prehensive monitoring strategies that include the sampling of both springs and wells (Quinlan, 1989) have been used to interpret geochemical variability that arises from ground-water flow through different parts of a carbonate aquifer system (Scanlon, 1990; Adamski, 2000).

Water samples were collected from 226 wells and 176 springs in seven carbonate aquifers from 1993 through 2003 as part of the U.S. Geological Survey's National Water-Quality Assessment Program. This number of samples from carbonate aquifers around the United States represents an opportunity to explore the differences in major-ion chemistry between samples collected from wells and from springs. Limestone and dolomite units were sampled within the following aquifers: Edwards-Trinity, Floridan, Mississippian, Basin and Range, Valley and Ridge, Springfield Plateau, and Ozark (fig. 1). These limestone and dolomite units range in age from Cambrian to Quaternary (Adamski, 2000; Miller, 1990; Maclay, 1995) and some are interlayered with sandstone or chert layers (Dettinger and others, 1995; Johnson, 2002; Kingsbury and Shelton, 2002).

COMPARISON OF SAMPLES FROM SPRINGS AND WELLS WITHIN SELECTED AQUIFERS

Spring and well water samples were collected from seven aquifers—Edwards-Trinity, Floridan, Mississippian, Valley and Ridge, Basin and Range,

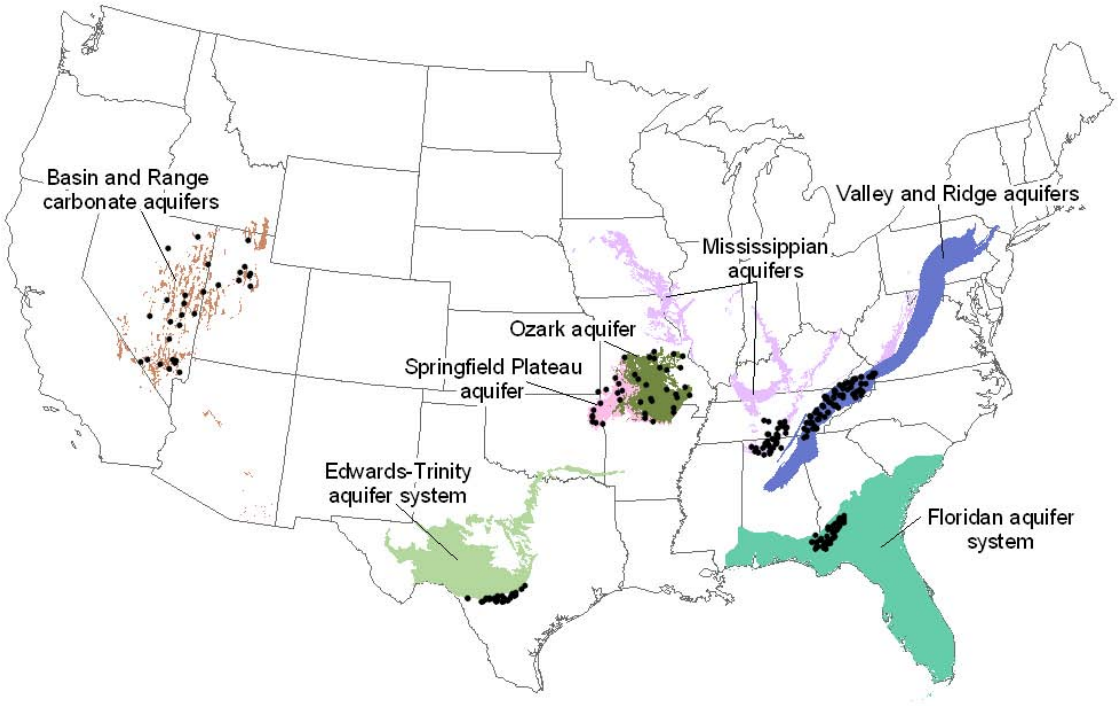

Figure 1. Location of spring and well sites sampled from 1993-2003.

Springfield Plateau, and Ozark. Within each aquifer, the number of water samples collected from springs ranged from 6 to 58 samples and the number of samples from wells ranged from 18 to 57 (fig. 2). In the Floridan aquifer system, samples were collected exclusively from the Upper Floridan aquifer, thus Upper Floridan will be used for the remainder of this discussion. Comparisons were made only between the water samples from springs and wells within a given hydrogeologic setting in each aquifer.

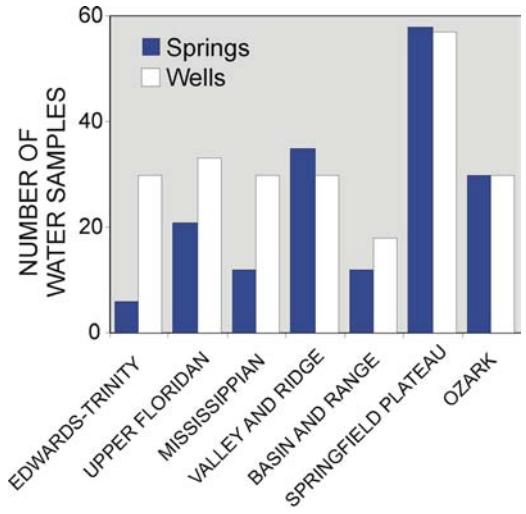

Figure 2. Number of spring and well samples collected from selected aquifers.

For example, in the Upper Floridan aquifer, samples were collected from throughout the extent of the aquifer, but spring water samples were collected only in southwestern Georgia; thus, these spring water samples were compared only to well samples collected in the same hydrogeologic setting in southwestern Georgia. The nonparametric Wilcoxon rank-sum test (Helsel and Hirsch, 1992) was used to determine if concentrations of constituents were significantly different (level of significance 0.05) between water samples collected from wells and springs.

Major Dissolved Species

Calcium-bicarbonate is the dominant water type for all of the aquifers and aquifer systems; however, the chemical composition of water samples from the springs and wells in the Basin and Range aquifer system was highly variable. In most aquifers, fewer than half of the 14 inorganic constituents examined showed significant differences in

Table 1. Summary of p-values from Wilcoxon rank-sum test comparing concentrations between samples from springs and wells.

[P-values lower than the level of significance, 0.05, are shaded gray; <, less than]

Aquifer	Calcium	Magnesium	Sodium	Potassium	Iron	Manganese	Bicarbonate	Sulfate	Chloride	Nitrate	Silica	pH	Dissolved oxygen	Dissolved solids
Edwards-Trinity	0.20	0.78	0.46	0.36	1.00	0.51	0.01	0.63	0.52	0.98	0.75	0.98	0.63	0.38
Upper Floridan	0.68	0.69	0.58	0.59	0.01	0.01	0.45	0.37	1.00	0.16	0.80	<0.01	0.12	0.52
Mississippian	0.70	0.61	0.05	0.72	0.14	0.44	0.74	0.38	0.08	0.36	0.18	0.11	<0.01	0.40
Valley and Ridge	0.36	0.18	0.17	0.06	<0.01	<0.01	0.16	0.01	0.29	0.09	0.10	0.08	<0.01	0.05
Basin and Range	0.08	0.85	0.25	0.44	<0.01	<0.01	0.25	0.24	0.92	0.98	1.00	0.09	0.66	0.25
Springfield Plateau	0.34	0.08	0.54	<0.01	0.33	0.10	<0.01	0.16	<0.01	<0.01	<0.01	<0.01	<0.01	0.05
Ozark	<0.01	<0.01	0.04	0.51	0.45	0.09	0.05	0.12	0.23	0.95	0.94	0.05	<0.01	<0.01

concentrations between springs and well samples (table 1). The greatest number of inorganic constituents with significant differences in concentration was seven in the Springfield Plateau aquifer. In three aquifers—Edwards-Trinity, Mississippian and Basin and Range—significant differences in concentrations were noted for only one or two properties, indicating that samples collected from springs and wells were collected from ground water from similar locations within the aquifer flow systems.

The range in dissolved solids concentrations among the seven aquifers provides some information about the relative residence times and flow path lengths in the aquifers. Aquifers with greatest median dissolved solids concentrations in spring and well samples, the Edwards-Trinity aquifer (322 and 294 milligrams per liter (mg/L), respectively) and the Basin and Range aquifer (410 and 364 mg/L, respectively), also had the greatest median well depths—1,270 feet (Edwards-Trinity) and 940 feet (Basin and Range). The median well depths for wells in the other aquifers ranged from 87 to 227 feet. Water from the deeper wells with greater dissolved solids concentrations may indicate that longer flow paths and older ground water are being sampled in these aquifers. Dissolved solids concentrations were only significantly different between spring and well samples in the Valley and Ridge and Ozark aquifers (fig. 3).

Median dissolved oxygen concentrations ranged from 2.5 mg/L in water samples from the Basin and Range aquifer wells to about 8 mg/L for springs in several of the aquifers (fig. 4). In four of the seven aquifers, dissolved oxygen concentrations were significantly different between samples from springs and wells (fig. 4). In each aquifer where significant differences in dissolved oxygen were noted, the spring samples have the greater dissolved oxygen concentrations, indicating generally younger waters and more dynamic flow systems. The median dissolved oxygen concentration in water samples from wells was greater than that for springs in the Edwards-Trinity aquifer. Deeper, more regional circulation of ground water may account for lower dissolved oxygen concentrations in some springs in the Edwards-Trinity aquifer.

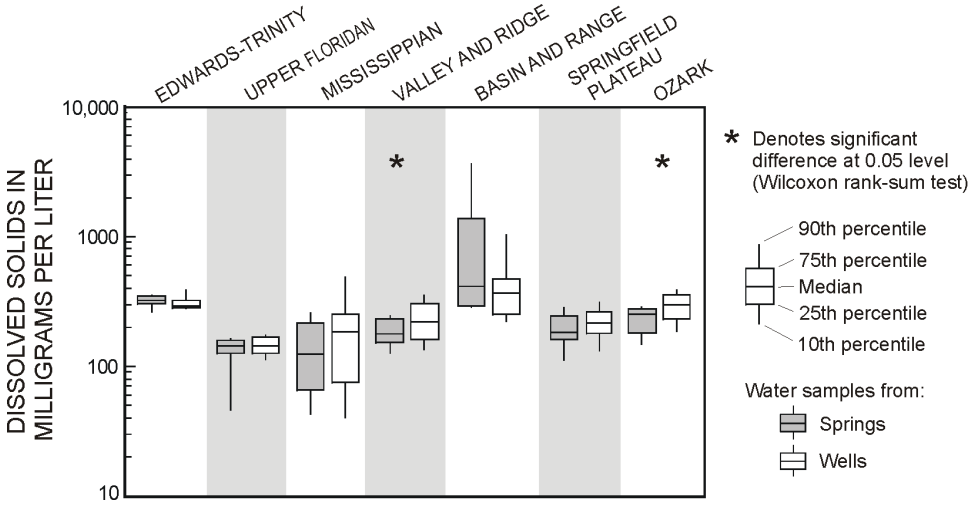

Figure 3. Distribution of dissolved solids concentrations in samples from springs and wells.

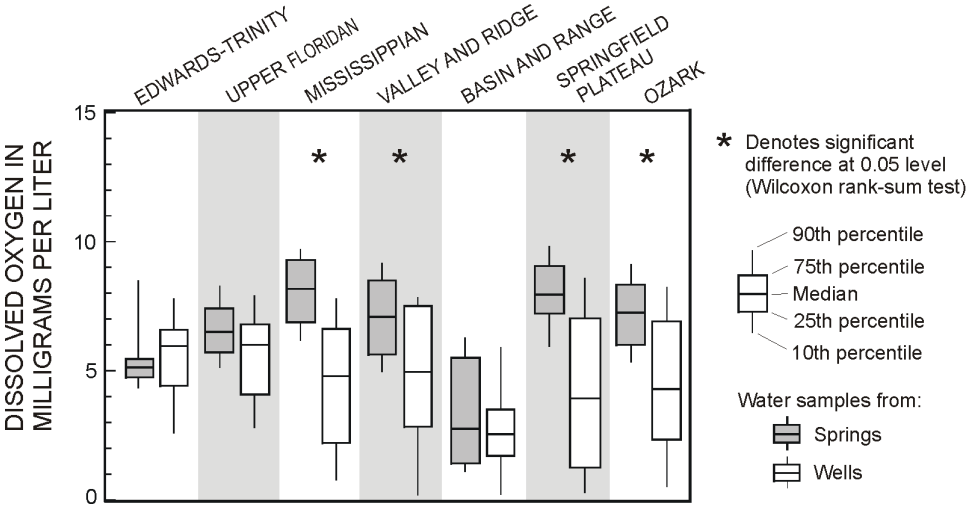

Figure 4. Distribution of dissolved oxygen concentrations in samples from springs and wells.

Saturation Indices with Respect to Calcite and Dolomite

Saturation indices were calculated for calcite and dolomite using the program PHREEQC (Parkhurst and Appelo, 1999). In most aquifers, the calcite saturation index values for the spring and well samples were at or near equilibrium (values of 0 +/- 0.2 are considered to represent equilibrium) (fig 5a). Most water samples were undersaturated with respect to calcite (values less than -0.2) for the Mississippian aquifer. Minerals in these aquifer materials may be less soluble than the aquifer materials in most of the other carbonate aquifers sampled.

Calcite saturation index values were significantly different between water samples from springs and wells in three of the seven aquifers—Upper Floridan, Springfield Plateau Ozark aquifers (fig. 5a). In each aquifer where the calcite saturation index values were significantly different (and in three of the other aquifers where significant differences were not noted), the significantly lower values were in the spring samples, indicating waters from

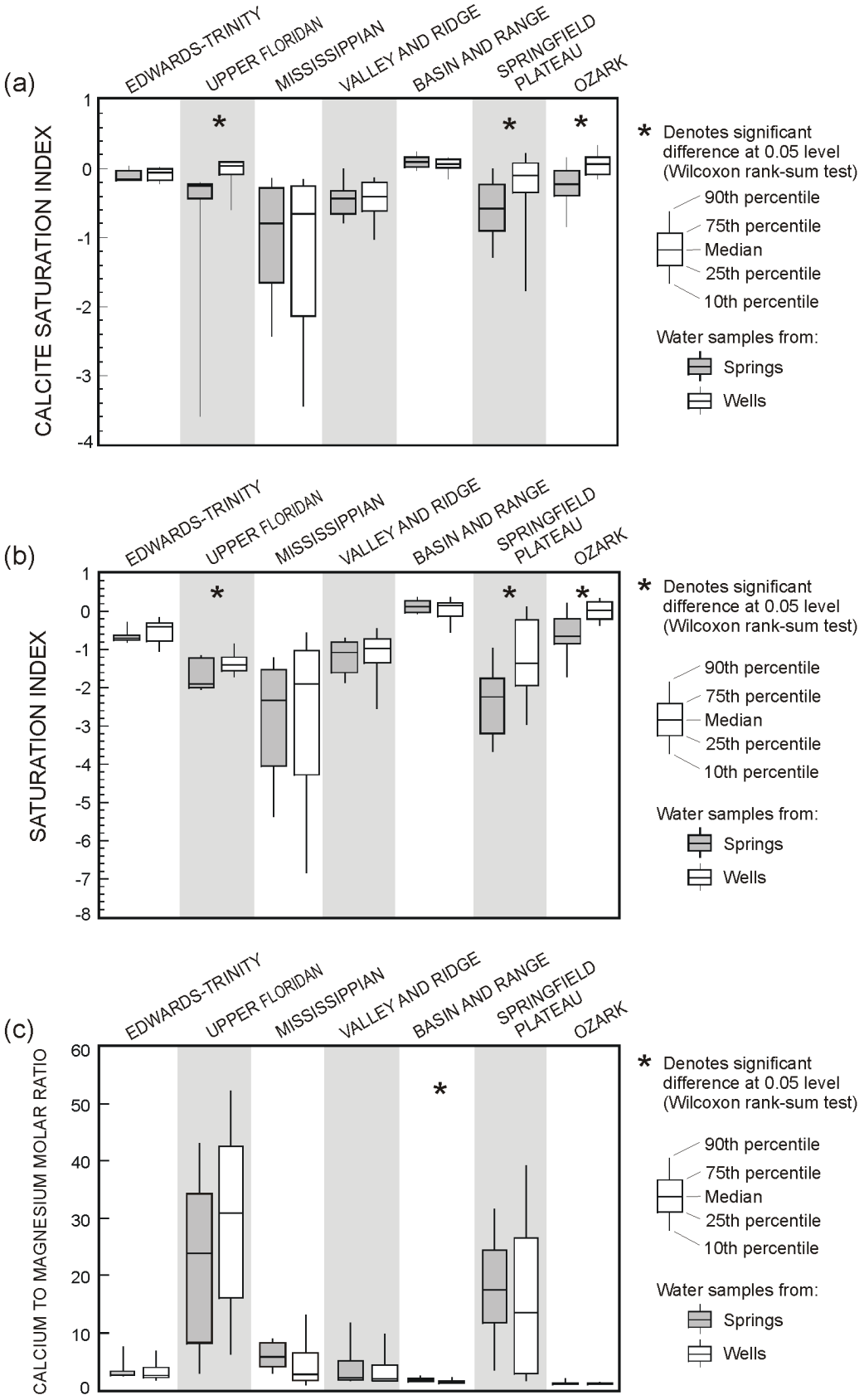

Figure 5. Distribution values for (a) calcite saturation index, (b) dolomite saturation index, and (c) calcium to magnesium molar ratio in samples from springs and wells.

springs were more undersaturated with respect to calcite than water from wells. The lower calcite saturation index values also indicate that spring waters may originate from shallower parts of the flow systems than the water withdrawn from wells.

Spring and well water samples for most of the aquifers were undersaturated with respect to dolomite (fig 5b). Only spring and well samples from the Basin and Range aquifer and well samples from the Ozark aquifer were at or near equilibrium with respect to dolomite (values mostly between -0.2 to 0.2) (fig 5b). Dolomite saturation index values for the spring and well samples were significantly different in three of the seven aquifers—Upper Floridan, Springfield Plateau, and Ozark (fig. 5b)—the same three aquifers where significant differences were noted for calcite saturation index values. In each of the three aquifers where dolomite saturation index values were significantly different (and in the four aquifers where significant differences were not noted), the significantly lower values were in the spring samples indicating that the spring samples were more undersaturated with respect to dolomite than the samples from wells.

The molar ratio of calcium to magnesium was calculated for each sample to determine if this ratio correlates with the relative amount of dolomite in the carbonate aquifers. Results show that in five of the aquifers, calcium-magnesium molar ratios were less than about 5, and are consistent with the reported mineralogy for the Edwards-Trinity, Mississippian, Valley and Ridge, Basin and Range, and Ozark aquifers (fig. 5c) (Maclay, 1995, Kingsbury and Shelton, 2002, Johnson, 2002, Dettinger and others, 1995, and Adamski, 2000). The three aquifers where the most dolomite is indicated (where the calcium-magnesium ratios were lowest), Edwards-Trinity, Basin and Range and Ozark aquifers, were also the aquifers where dolomite saturation index values were highest (greater than -1.0) (figs. 5b and 5c).

Nitrate

Median nitrate concentrations in the seven aquifers ranged from 0.32 to 2.5 mg/L (fig. 6). Median concentrations were lowest (less than 1.0 mg/L) in the spring and well water samples from the Basin and Range and the Ozark aquifers. Although median nitrate concentrations did not exceed the maximum contaminant level of 10 mg/L, several median nitrate concentrations ranged from 1 to 4 mg/L, which may indicate anthropogenic inputs. Nitrate concentrations were only significantly different between spring and wells samples in the Springfield Plateau aquifer. The significantly higher concentrations in nitrate in water samples from springs relative to wells in the Springfield Plateau was noted by Adamski (2000) who attributed the higher nitrate concentrations to the greater susceptibility of

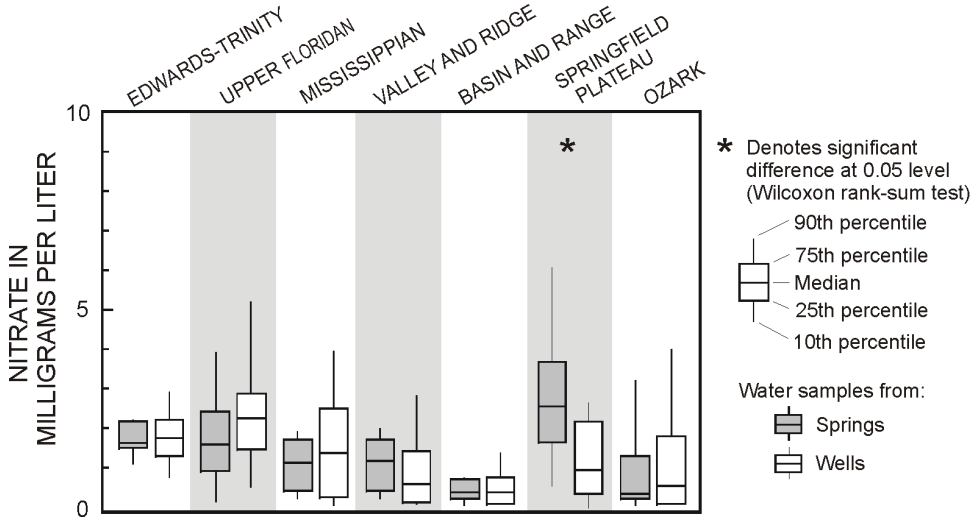

Figure 6. Distribution of nitrate concentrations in samples from springs and wells.

springs to surface sources of contamination. The land use in the area overlying the Springfield Plateau aquifer is predominantly agriculture (Adamski, 1996).

IMPLICATIONS FOR USE OF SPRINGS IN THE CHARACTERIZATION OF WATER QUALITY IN CARBONATE AQUIFERS

Differences in chemistry between spring waters and well water reflect ground-water movement in distinct parts of the flow system. Higher dissolved oxygen concentrations, lower saturation indices with respect to calcite and dolomite, and lower dissolved solids concentrations relative to water from wells, indicate that springs discharge ground water mainly from shallow parts of most of the studied aquifer systems. Exceptions are the Basin and Range and the Edwards-Trinity aquifers, where deeper circulation of ground water may occur prior to discharge from springs. Chemical differences between water from springs or wells also are related to the hydrologic conditions at the time of sampling. Rainfall patterns should be evaluated along with spring discharge at the time of sampling to characterize the contribution of recent recharge to the aquifer and its impact on ground-water chemistry.

There were no consistent patterns when comparing nitrate concentrations in spring waters and well water. Nitrate concentrations were significantly higher in spring water than in ground water in the Springfield Plateau aquifer, but not in the adjacent Ozark aquifer. Nitrate concentrations were higher in spring waters than in well waters from the Valley and Ridge aquifer, but nitrate concentrations in spring waters were similar or lower than nitrate concentrations in well waters from the Edwards-Trinity, Upper Floridan, Mississipian, and Ozark aquifers. These differences likely reflect the complex relation between nitrate concentrations in ground water and various nitrogen sources, and include past and present land-use and waste-management practices, and hydrologic and climatic variability.

Spring samples most likely represent water from shallower parts of the aquifer flow systems, and flow through large solution openings in carbonate aquifer systems. These parts of the flow system are also the parts of the aquifer systems most susceptible to contamination from land-use practices. For these reasons, obtaining water samples from springs, in addition to wells, may be necessary for adequate characterization of water quality in carbonate aquifers and for addressing their susceptibility to contamination.

REFERENCES

Adamski, J.C., 1996, Nitrate and pesticides in ground water of the Ozark Plateaus region in Arkansas, Kansas, Missouri, and Oklahoma: U.S. Geological Survey Fact Sheet FS-182-96, 4 p.

Adamski, J.C., 2000, Geochemistry of the Springfield Plateau aquifer of the Ozark Plateau Province in Arkansas, Kansas, Missouri, and Oklahoma, USA: Hydrological Processes, vol. 14, p. 849-866.

Dettinger, M.D., Harrill, J.R., Schmidt, D.L., and Hess, J.W., 1995, Distribution of carbonate-rock aquifers and the potential for their development, southern Nevada and adjacent parts of Arizona, California, and Utah: U.S. Geological Survey Water-Resources Investigations Report 91-4146, 100 p.

Helsel, D.R., and Hirsch, R.M., 1992, Statistical methods in water resources: New York, Elsevier, 522 p.

Johnson, G.C., 2002, Water quality of springs in the Valley and Ridge Physiographic Province in the Upper Tennessee River Basin, 1997: U.S. Geological Survey Water-Resources Investigations Report 02-4180, 24 p.

Kingsbury, J.A., and Shelton, J.M., 2002, Water quality of the Mississippian carbonate aquifer in parts of middle Tennessee and northern Alabama, 1999: U.S. Geological Survey Water-Resources Investigations Report 02-4083, 36 p.

Maclay, R.W., 1995, Geology and hydrology of the Edwards aquifer in the San Antonio Area, Texas: U.S. Geological Survey Water-Resources Investigations Report 95-4186, 64 p.

Miller, J.A., 1990, Ground water atlas of the United States, Segment 6, Alabama, Florida, Georgia, and South Carolina: U.S. Geological Survey Hydrologic Investigations Atlas 730-G, 28 p.

Parkhurst, D.L., and Appelo, C.A.J., 1999, User's Guide to PHREEQC (Version 2)--A Computer Program for Speciation, Batch-Reaction, One-Dimensional

Transport, and Inverse Geo-chemical Calculations. U.S. Geological Survey Water-Resources Investigations Report 99-4259, accessed at http://www-brr.cr.usgs.gov/projects/GWC_coupled/phreeqc/html/final.html, on June 2, 2005.

Quinlan, J.F., 1989, Ground-water monitoring in karst terranes: Recommended protocols and implicit assumptions: U.S. Environmental Protection Agency Report EPA/600/X-89/050, 79 p.

Scanlon, B.R., 1990, Relationships between groundwater contamination and major-ion chemistry in a karst aquifer. Journal of Hydrology, 119, p. 271-291.

Interpretation of Water Chemistry and Stable Isotope Data from a Karst Aquifer According to Flow Regimes Identified through Hydrograph Recession Analysis

By D. H. Doctor[1] and E. C. Alexander, Jr.[2]
[1] U.S. Geological Survey, 345 Middlefield Rd., MS 434, Menlo Park, CA, 94025
[2] Univ. of Minnesota, Dept. of Geology and Geophysics, 310 Pillsbury Dr. SE, Minneapolis, MN, 55414

ABSTRACT

In this study the relation between flow regime and chemistry of a major karst groundwater resurgence zone in southwestern Slovenia was examined using spring hydrograph recession analysis. Long-term (>2 weeks) recession periods were isolated from 6 years of flow data. Breaks in slope on a plot of the natural log of the discharge versus time allowed for the identification of four separate flow regimes of the aquifer outflow. Major ion chemistry and stable isotopic composition ($\delta^{18}O$ of water and $\delta^{13}C$ of DIC) of samples collected twice monthly for two years were then grouped according to where they had been collected within each identified flow regime. Patterns in the chemical and isotopic data emerged which indicated shifting sources of water contributing to the outflow of the spring under different hydrologic conditions. This type of analysis may be a valuable water resource management tool in other karst regions.

INTRODUCTION

A primary challenge for the management of karst water resources is to characterize water quality changes with discharge variability. In order to accomplish this goal, managers must be able to efficiently assess two aspects of the karst aquifer system that interact and determine overall water quality: the hydrologic and the hydrochemical variability. Often, however, resources for characterizing water quality across the full range of hydrologic variability are limited, resulting in a frequency of water sampling that is far lower than the actual time scale of chemical changes taking place at the point of measurement. Therefore, a need exists for a method through which relatively infrequent water quality data can be used to accurately understand and possibly predict major changes in water quality as the hydrologic conditions change.

In this paper, we describe a technique in which long-term records of discharge and relatively infrequent water quality sampling can be combined for the purpose of studying water quality changes with flow. The steps are not mathematically complex, allowing for straightforward and rapid culling of information from data which already exists for many springs. The analysis begins with examination of the recession limbs of a long-term (several years) record of discharge. First suggested by Maillet (1905), several authors have since proposed that the recession limb of a karst spring hydrograph can be approximated by a function that is the sum of several exponential segments of the total recession (Forkasiewicz and Paloc, 1967; Hall, 1968, Milanović, 1981; Bonacci, 1993; Tallaksen, 1995). Thus, the entire discharge-time relationship of the recession is expressed as:

$$Q(t) = \sum_{i=1}^{N} q_0^i e^{-(\alpha_i)t}. \qquad \text{(eq, 1)}$$

Where Q is the discharge at time t, N is the number of exponential segments of the recession, q_0^i is the discharge at the beginning of each recession segment, and α_i is the recession coefficient for each segment. In this model, each exponential segment is interpreted to represent the depletion of an aquifer reservoir, with the rate of depletion of that reservoir being represented by the recession coefficient (α_i). Accordingly, the segment with the greatest recession coefficient would represent the most rapid drainage of the karst network (presumably surface runoff or displacement of water into the largest conduits) and the recession segment with the smallest coefficient would represent the baseflow (i.e., the slow drainage of that portion of the aquifer with the lowest transmissivity). The latter is often termed the *diffuse flow*

portion of the aquifer, while the most transmissive conduits are referred to as the *quickflow* portion of the aquifer. Intermediate segments of the total hydrograph recession are thought to represent the emptying of aquifer volumes having intermediate values of hydraulic conductivity.

In reality, it is not clear whether the above conceptual interpretation has any definitive physical validity. It is extremely difficult to quantify the proportions of various transmissive elements of a karst aquifer given the high degree of heterogeneity in karst. Moreover, the conceptual model of a karst aquifer having separate "diffuse flow" and "quickflow" components may be misleading, as the physical connectivity between fractures and solutionally enlarged conduits exists more as a continuum of transmissivities within the aquifer. Nonetheless, the full recession of the hydrograph contains much useful information, particularly concerning (1) the volume of water drained from the system over time after peak flows, regardless of where the flow originates in the body of the aquifer, and (2) changes in the rate of discharge that occur at discrete values of discharge, thus placing quantifiable limits on aquifer flow regimes.

Constructing a Master Recession Curve

Assuming individual recession segments can be identified, the mean values of q_o and α for each segment can be used to construct a Master Recession Curve (MRC) of the spring or well (in the absence of identifiable linear segments on a semi-log plot of discharge vs. time, other models may be applied to estimate the segments of the MRC; see Sujono and others, 2004 for examples). Each segment of the MRC is only a portion of an individual exponential recession curve, the constants of which are defined by the values of the recession constant (α) and the initial discharge defining the upper limit of the recession segment (q_o). Taken individually, each of these curves represents aquifer drainage under a particular flow regime, defined by the discharge measured over a specified time interval after the onset of the recession. Except for the tail end of the baseflow recession curve, the time intervals of all of the recession segments overlap. Thus, the volumes of water contributed by the underlying curves must be accounted for as part of the volume of water drained solely by an individual segment.

For example, let us assume an arbitrary master recession curve of a karst spring, represented in semi-log space in **Figure 1**. Three exponential recession curves ($Q_f(t)$=fast flow, $Q_i(t)$=intermediate flow and $Q_b(t)$=baseflow) combine to give the overall recession, which is represented by the uppermost surface of the intersecting lines shown in Figure 1. The total volume of water drained across the fast flow portion of the recession is equivalent to the integration of recession curve $Q_f(t)$ on the interval t_o to t_i. In this way, the calculation sums together the volumes V_f^f , V_i^f and V_b^f. Lacking any *a priori* knowledge of the physical significance of these volumes for the functioning of the aquifer, their estimation may not seem consequential. However, for the purposes of water quality interpretation it may be desirable to separate the fastest flow portion from the other volumes drained across the MRC. Thus, we may calculate the fast flow volume (V_F) determined solely by the largest recession constant (α_f) and separated from the baseflow and intermediate flow volumes as:

$$V_F = V_f^f = \int_{t_0}^{t_i} Q_0 \exp(-\alpha_f t)\,dt - \int_{t_i}^{t_i} q_0^i \exp(-\alpha_i t)\,dt \quad \text{(eq. 2)}$$

By integrating the MRC only on the interval from the time of peak flow until the break in slope and intersection with the next recession curve, the expression in eq. 2 quantifies the volume drained solely under the fastest draining portion of the MRC; it is only the volume of the fast flow regime that we seek to define. The "fast flow" volume is not equivalent to the total theoretical volume drained by the uppermost recession curve—rather, it is a flow regime we are defining independent of (but dominated by) that recession curve. The fast flow regime thus includes theoretical contributions from all 3 recession segments.

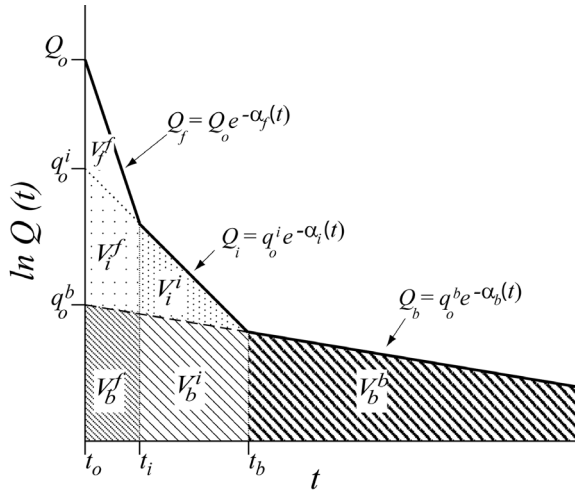

Figure 1. Schematic representation of a Master Recession Curve (MRC) and the theoretical drainage volumes obtained by integration beneath individual linear segments (see text for details).

portion of the MRC; it is only the volume of the fast flow regime that we seek to define. The "fast flow" volume is not equivalent to the total theoretical volume drained by the uppermost recession curve—rather, it is a flow regime we are defining independent of (but dominated by) that recession curve. The fast flow regime thus includes theoretical contributions from all 3 recession segments.

Similarly, the intermediate flow (V_I) and baseflow (V_B) volumes (represented in Figure 1 by the stippled region and cross-hatched region, respectively) can be calculated by the following equations:

$$V_I = \int_{t_0}^{t_b} q_0^i \exp(-\alpha_i t)dt - \int_{t_0}^{t_b} q_0^b \exp(-\alpha_b t)dt \qquad \text{(eq. 4)}$$

$$V_B = \int_{t_0}^{t_\infty} q_0^b \exp(-\alpha_b t)dt \qquad \text{(eq. 5)}$$

Thus, the total volume of water, V_T drained across the entire recession, from t=0 to t=∞ is:

$$V_T = V_F + V_I + V_B. \qquad \text{(eq. 6)}$$

Using these expressions to quantify theoretical volumes of outflow for a particular spring, one may now look to characterize the quality of water drained from those volumes based upon chemical and/or isotopic data. This was the approach taken for the case study described herein.

STUDY SITE AND BACKGROUND

This study was conducted within the Classical Karst, located along the border between southwestern Slovenia and northeastern Italy. The Slovene name for this region is *Kras*, and this term will be used hereafter in order to signify the geographic location. The Kras region is an uplifted, overturned anticlinal block of Cretaceous limestone forming a plateau at approximately 400 m above sea level. The Kras region is 40 km long, up to 13 km wide, and covers approximately 440 km^2, with mean annual precipitation between 1400 and 1600 mm (Kranjc, 1997). Rainfall easily infiltrates into the limestone bedrock, due to thin soil thickness (0 to 0.5 m) and the abundance of bare karst bedrock surfaces. No surface streams exist on the Kras plateau. Given the abundant annual precipitation, highly permeable land surface, and lack of surface water runoff, autogenic recharge on the Kras surface is a major component of recharge to the underlying aquifer.

In the past, hydrogeological research on the Kras focused mainly on the source of water of the Timavo springs. The Timavo springs are the largest natural source of groundwater in the region, and have been an object of curiosity for centuries (Galli, 1999). The largest of these springs has been dived to a depth greater than 80 m below sea level, where phreatic conduits of diameters in the tens of meters have been mapped (Guglia, 1994). Collectively, the long-term average discharge of the springs is approximately 30.2 m^3/sec (variable within the years studied between 18 m^3/sec and 39.4 m^3/sec), with low flows averaging around 9 m^3/sec, and maximum flows over 130 m^3/sec (Gemiti, 1984).

The Timavo springs represent the major component of outflow (85%) of the regional karst groundwater system (Civita and others, 1995). Several other springs in proximity to the Timavo springs form the remainder of the groundwater resurgence zone. Of these, Sardos spring and Moschenizze North spring are also reclaimed for water supply.

These springs, as well the water from a supply well (B-4) and a monitoring well (B-3) were sampled in this study (**Figure 2**). The water supply well B-4 provides the sole water source for the inhabitants of the Kras region in Slovenia, serving a population of approximately 25,000 people. The monitoring well B-3 is completed within a zone of fluctuating water level, and was observed to be dry after a drought period. Samples collected from the well before and after the drought exhibited nearly identical water chemistry; thus, this well contains water that is displaced from storage within the local vadose zone. A large river, the Soca River, drains the high Julian Alps along the western border between Italy and Slovenia. This river loses a large amount of flow into the karst aquifer (20 m^3/sec), and is believed to account for much of the flow from the springs in

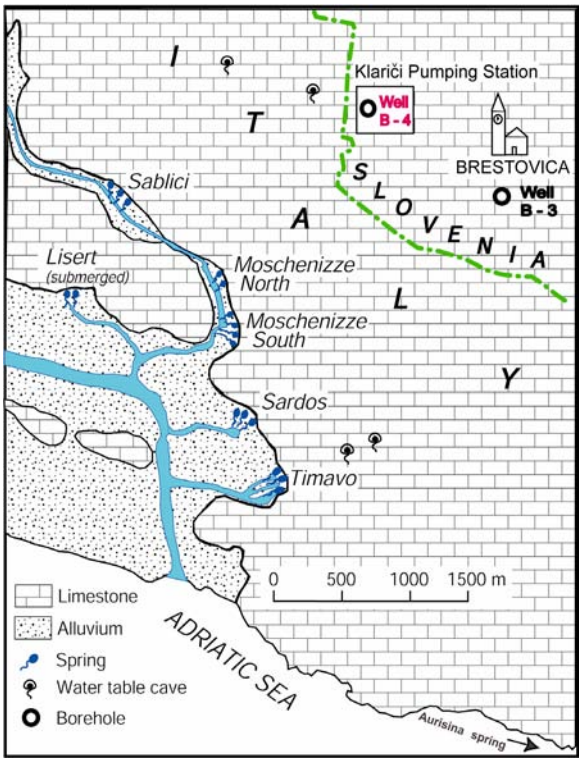

Figure 2. The groundwater resurgence zone of the Kras region (after Krivic, 1981).

the summer (Mosetti & D'Ambrosi, 1963; Urbanc & Kristan, 1998). The primary goal of this study was to determine how the contribution from the Soca River affects the outflow of the springs with changing flow conditions.

Daily discharge measurements exist at the Timavo springs as a consequence of their reclamation for water use. In order to quantitatively define the flow regimes considered here, a hydrograph analysis of the Timavo springs discharge was performed. Six years of discharge records were available, from 1995-2000. Out of the six-year record, six of the longest recession periods were chosen for detailed analysis. The recession flows at the Timavo springs were fit by a series of linear segments of the hydrograph recession in semi-log space. The simple exponential decay relation (*eq. 1*) appears to provide an adequate model for the analysis of all discharge regimes at the springs.

METHODS

From our hydrograph recession analysis, a Master Recession Curve (MRC) (**Figure 3**) was constructed. Individual storm event recessions from the long-term discharge records of the Timavo springs were compiled to form the MRC. Four distinct segments to the Timavo MRC were identified, each corresponding to a characteristic flow regime. The breaks in slope define the approximate discharge limits of each flow regime.

The MRC construction was performed manually by visual inspection of the individual event hydrographs. Individual event recession periods were isolated from the entire discharge record and were plotted as the natural log of the flow (ln *Q*) vs. time (*t*). **Figure 4** shows one of these recession hydrographs of the Timavo springs. Linear ordinary least-squares regression lines were then fit to each segment of each event hydrograph in semi-log space. The slopes of the regression lines are equal to the values of the recession coefficient (α) for each flow regime of the MRC in units of day^{-1}, and the y-intercept of the regression lines are the value of discharge at the start of the recession (q_o at t=0). The values of α and q_o that were obtained from the linear regressions of the six event hydrographs were tabulated for each segment of each event, and averaged. These results are presented in **Table 1**.

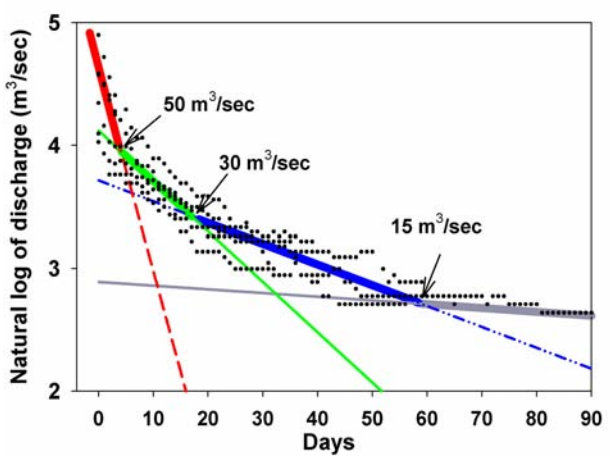

Figure 3. Master Recession Curve for the Timavo springs. Lines indicate ordinary least-squares regression through recession segments. Average daily discharge data are shown as dots.

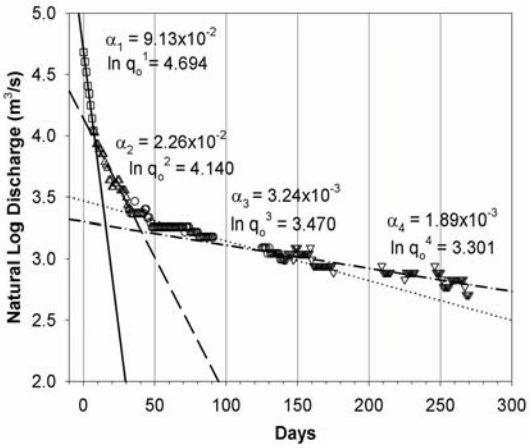

Figure 4. Representative recession hydrograph of the Timavo springs.

Since it was a common occurrence that recession segments would be cut off by increases in discharge resulting from new recharge events, the values of α and q_o were weighted according the time duration of each segment prior to an increase in discharge. Thus, values of α and q_o obtained from individual recessions that persisted for longer time periods were more heavily weighted in the calculation of the mean values for that portion of the MRC. This practice lends a deliberate bias towards the larger events; the largest events recharge a greater portion of the vadose zone as the water table of the aquifer rises, thus they produce longer, more informative, recessions.

A limitation to the analysis in this case is that the Timavo springs, having been engineered for water reclamation, are fitted with a sluice gate that controls the discharge at low flow. The consequence of the control structures is that the baseflow never drops below 9 m^3/sec. Thus, the true baseflow recession slope may be absent. Nonetheless, significantly long periods of recession that were not influenced by the control structures were observed such that reproducible recession segments could be fit to the discharge record.

RESULTS AND DISCUSSION

Four flow regimes of the Kras aquifer were defined through the hydrograph analysis: (1) flood flow, (2) high flow (3) moderate flow, and (4) baseflow. The flood flow regime is for flows of the Timavo springs above approximately 50 m^3/sec, high flow is between 30 and 50 m^3/sec, moderate flow is between 15 and 30 m^3/sec, and baseflow discharge is below 15 m^3/sec.

The individual segments of the MRC were integrated to provide an area below the curve that represents the total theoretical storage volume of the aquifer that supplies the discharge of the Timavo springs. These results are shown in **Table 1**.

Comparison between flow regimes, isotopes, and chemistry

The isotopic and chemical data collected in this study were grouped into the four flow regimes according to the discharge measured at the Timavo springs on the date the water sample was collected. Oxygen ($\delta^{18}O$ of water) and carbon ($\delta^{13}C$ of dissolved inorganic carbon, or $\delta^{13}C_{DIC}$) stable isotope data of the Timavo springs collected between November 1998 and November 2000 were grouped together by flow regime, and box plots were constructed.

TABLE 1. Results of Timavo springs hydrograph recession analysis

Recession segment	Flow regime	Discharge range (m^3/sec)	α (day^{-1})	q_o (m^3/s)	Recession Period (days)	Storage volume (m^3)	% of total storage
1	Flood flow	> 50	1.64×10^{-1}	101.49	0 (peak Q) – 4	0.06×10^8	1.0%
2	High flow	30 to 50	4.10×10^{-2}	61.56	4 – 17	0.13×10^8	2.2%
3	Moderate flow	15 to 30	1.70×10^{-2}	40.98	17 – 58	0.48×10^8	8.2%
4	Baseflow	<15	3.00×10^{-3}	18.00	58 or more	5.18×10^8	88.5%
					Total:	5.85×10^8	100 %

The relation between $\delta^{18}O$ and flow regime is opposite to the relation between $\delta^{13}C_{DIC}$ and flow regime (**Figure 5a & 5b**). The $\delta^{18}O$ values become more negative with higher flow while $\delta^{13}C_{DIC}$ values become more positive. The increase in $\delta^{18}O$ and corresponding decrease in $\delta^{13}C_{DIC}$ with increasing flow is consistent throughout the sampling period. In addition, similar seasonal trends are apparent among the isotopic variation of all of the groundwaters (**Figure 6**). Note that all the groundwaters can be approximated as a mixture between the water of well B-3 (autogenic recharge) and the Soca River.

The high-altitude (>2000 m) alpine source of the Soca River lends it $\delta^{18}O$ values that are more negative than the water derived from local rainfall on the Kras. The $\delta^{18}O$ of weighted mean annual precipitation is -6.5‰, essentially equal to the composition of well B-3. Thus, the difference in $\delta^{18}O$ between these sources of water allows for discrimination between them in the mixtures of the groundwaters.

Similarly, the difference in $\delta^{13}C_{DIC}$ values between the Soca River and autogenic recharge (represented by the composition of well B-3) adds a second parameter by which to discriminate between these sources in the outflow. Lower $\delta^{13}C_{DIC}$ values in the autogenic recharge water reflect a greater proportion of DIC derived from soil CO_2, which tends to be low in $\delta^{13}C_{DIC}$ as a result of the oxidation of organic matter (Deines, 1980; Deines and others, 1974). The partial pressure of CO_2 in the unsaturated zone is 10-100 times that of the atmosphere with $\delta^{13}C$ values between -20 and -25‰ (Doctor, 2002), thus lower $\delta^{13}C_{DIC}$ values indicate water that has been stored within the vadose zone of the karst.

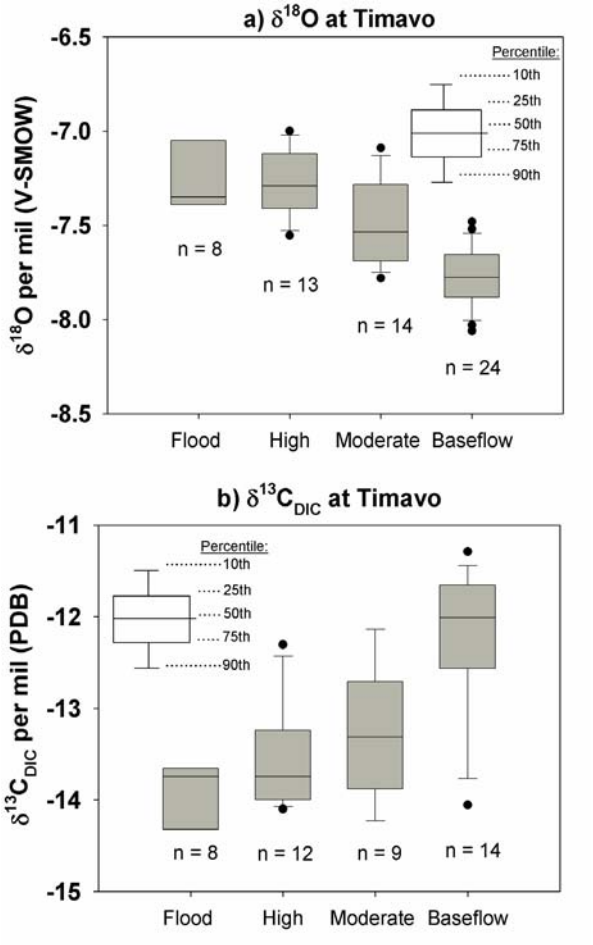

Figure 5. Changes in stable isotopic composition with flow regimes at the Timavo springs. Outlier values correspond to samples collected immediately after or during storm events.

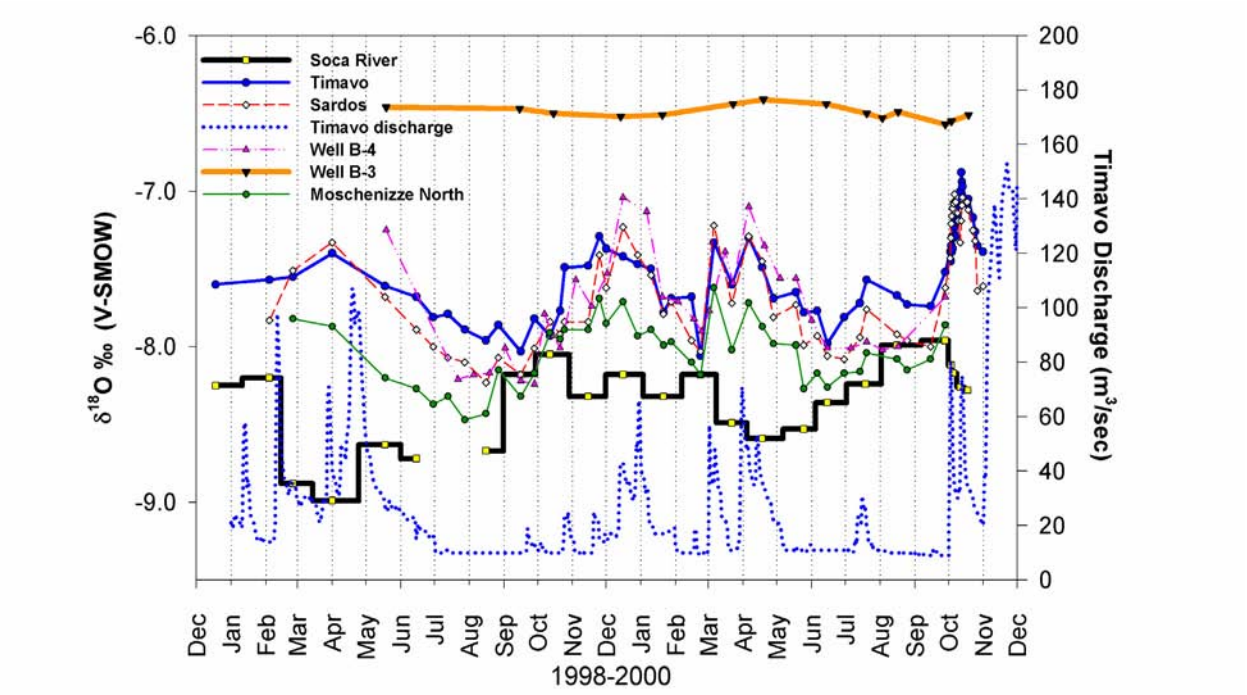

Figure 6. Time series of oxygen isotope values of the Kras groundwaters, with the average daily discharge of the Timavo springs shown for reference. Note that all the groundwaters are a mixture between the water of well B-3 (autogenic recharge) and the Soca River.

Together, these isotopic data present a conceptual model of two component mixing between allogenic Soca River water and autogenic recharge from local precipitation to account for the observed isotopic compositions of the Kras groundwaters. The proportion of Soca River water issuing from the springs is apparently greatest under lower flow conditions, while increasing amounts of autogenic recharge water are released from storage in the vadose zone during higher flows.

The chemistry data from the present study was combined with the chemistry data of Gemiti & Licciardello (1977) and of Cancian (1987), assuming similarity between the flow regimes determined by those authors and the flow regimes determined by the recession analysis of the present study. For the combined chemistry data it was possible to characterize only three flow regimes, since Cancian (1987) reports only three in his data summary. Therefore, the mean values of the flood flow and high flow regime from the recession analysis were combined into "high flow", and the baseflow values are defined as "low flow".

The results of the water chemistries grouped according to flow regime are shown in **Figures 7 to 9. Figure 7** shows the Ca/Mg ratios of all the groundwaters tend to approach that of the Soca River as the flow decreases with the exception of well B-4, which shows a relatively constant Ca/Mg ratio regardless of flow regime. Of the other springs, Timavo has the highest Ca/Mg values, followed by Sardos and then by Moschenizze North. Well B-3 has a much higher and constant Ca/Mg than the other waters, thus the progressive shift toward higher Ca/Mg values with increasing flow regime implies a shift toward a greater proportion of autogenic recharge water supplying the springs.

For Cl^-, all of the groundwaters show similar concentrations except for well B-4, which has the highest Cl^- concentrations of all of the groundwaters (**Figure 8**). Cl^- levels in the other groundwaters are relatively constant at 5-10 ppm across the flow

regimes, while for well B-4 the Cl^- is highest at high flow (>50 ppm on average) and decreases to approximately 20 ppm on average at low flow. Well B-3 has a low and constant Cl^- concentration of 3.0 ppm.

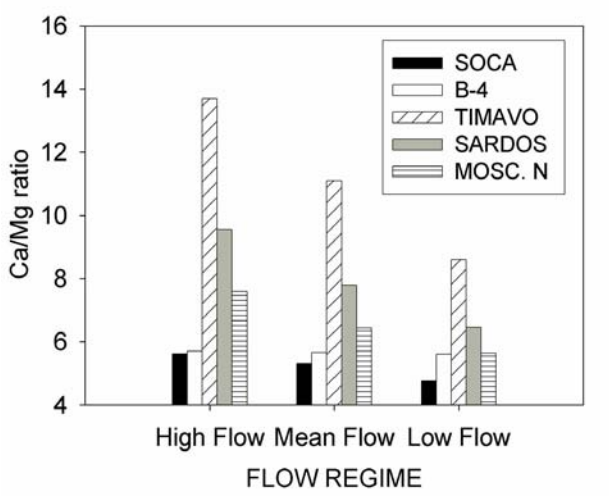

Figure 7. Ca/Mg ratio of Kras groundwaters with flow regime.

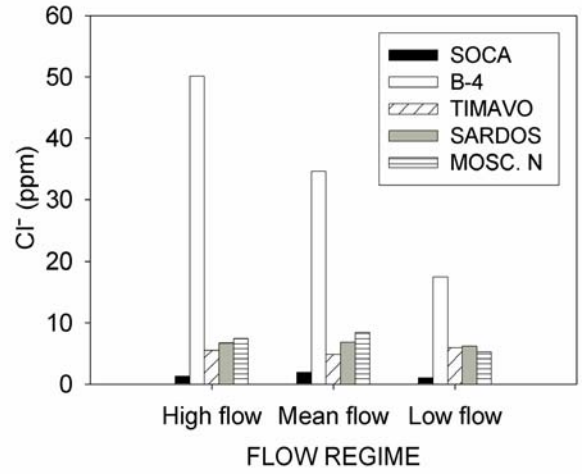

Figure 8. Cl^- of Kras groundwaters with flow regime.

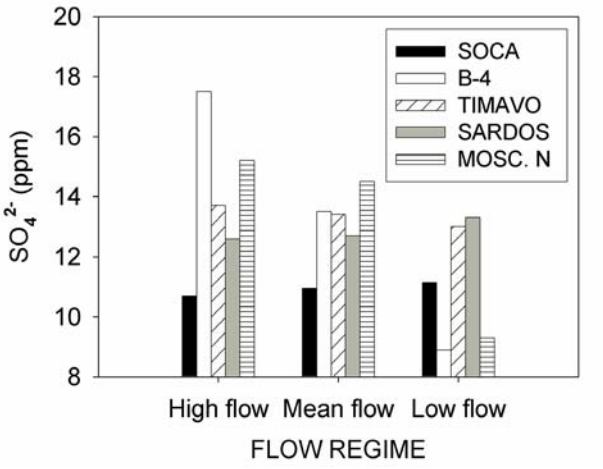

Figure 9. SO_4^{2-} of Kras groundwaters with flow regime.

Well B-4 also shows anomalous chemistry with respect to SO_4^{2-}; it has the highest SO_4^{2-} concentrations of all the groundwaters at high flow and the lowest SO_4^{2-} at low flow (**Figure 9**). SO_4^{2-} concentrations at Timavo and Sardos stay relatively constant regardless of flow regime, at between 12-14 ppm on average. SO_4^{2-} at well B-4 and Moschenizze North decreases with decreasing flow regime, and at low flow they exhibit the lowest SO_4^{2-} concentrations of all the groundwaters.

High chloride (>100 ppm) and sulfate (>30 ppm) concentrations have been observed from two shafts intersecting the water table nearby the Timavo springs (Gemiti, 1994). The water in these shafts is derived from local storage of autogenic recharge within the epikarst, and may be influenced by anthropogenic activities. This water stored within the unsaturated zone impacts well B-4 and Moschenizze North spring under elevated hydraulic head conditions, and to a lesser extent at low flow. Because these two sites exhibit higher Cl^- and SO_4^{2-} when the water table rises, it is likely that an overflow connection permits the higher salinity water to affect both well B-4 and, to a lesser degree, Moschenizze North spring under high flow conditions.

CONCLUSIONS

Hydrochemical and isotopic data collected at a frequency of approximately twice monthly over a two-year period was interpreted through identification of discrete flow regimes of the karst aquifer by means of hydrograph recession analysis. Grouping the chemistry data together within the defined flow regimes illuminated broad patterns of water quality variability according to changing discharge conditions.

The simple exponential decay model used for fitting multiple linear recession segments to the outflow of the Timavo springs was adequate for determining the flow regimes of the groundwater resurgence of the Slovene Kras region. As a result of the recession analysis, four distinct flow regimes of the Timavo springs have been defined: flood flow (>50 m^3/s), high flow (30–50 m^3/s), moderate flow (15–30 m^3/s), and baseflow (<15 m^3/s). The estimated storage volume of the baseflow regime represents the greatest proportion (88.5%) of the total theoretical storage volume, with the flood and high flow regimes together representing 3.2%. These percentages highlight the importance of the baseflow regime for providing the majority of flow at the Timavo springs. Although high flows do not drain those portions of the aquifer with a large capacity for water storage, floods are responsible for recharging other parts of the aquifer system, thus flood waters may remain in storage for longer periods of time than otherwise may be indicated by the rapid drainage under higher flow regimes.

The flow at the Timavo springs serves as an adequate proxy for the flow of the other local springs that drain the aquifer. Similar trends in the stable isotopic composition ($\delta^{18}O$ and $\delta^{13}C_{DIC}$) of the water exist among the Timavo springs, Sardos spring, and well B-4 when compared to the discharge of the Timavo springs. For each of these groundwaters, the $\delta^{18}O$ values are lowest during lowest flow periods and highest during the highest flow periods, while the $\delta^{13}C_{DIC}$ values are lowest during high flow and highest during low flow. These results indicate mixing between similar sources at each of these outflow points, as well as a change in the proportions of each source under changing hydrologic conditions. The more negative $\delta^{18}O$ and more positive $\delta^{13}C_{DIC}$ values of the waters are consistent with a predominant Soca River source during low flow periods, while the more positive $\delta^{18}O$ and more negative $\delta^{13}C_{DIC}$ values are consistent with a predominant source of storage within the vadose zone.

The relations among the flow regimes and water chemistry are similar to the results previously reported by Gemiti and Licciardello (1977) and Cancian (1987). There is a general trend of decreasing Ca/Mg ratio with decreasing flow regime in all of the groundwaters sampled, except for well B-4. Since the Soca River shows the lowest Ca/Mg ratio of all the waters, and autogenic recharge water (well B-3) shows the highest Ca/Mg ratio, the decreasing trend supports the conclusion of variable mixing between the Soca River and autogenic recharge such that under lower flow conditions Soca River water has a greater influence on the groundwater of the aquifer.

The anomalous Cl^- and SO_4^{2-} chemistry observed at the Klarici supply well (well B-4) indicates a high salinity component that affects this well when phreatic head levels are elevated during high flows. Water chemistries of local vadose shafts indicate that the source of this high salinity water is likely a shallow perched zone of water in storage within the epikarst. This water may be anthropogenically impacted.

The trends observed in both isotopic and chemical composition of the groundwaters as flow regimes change indicate that pronounced shifts in the water sources feeding the groundwaters of the Kras aquifer resurgence zone occur as hydrologic conditions vary. These data show that under low flow conditions the outflow contains a greater proportion of Soca River water, while under high flow conditions more water discharged from the springs is derived from the vadose zone. In addition, a third source of water with high levels of Cl^- and SO_4^{2-} exists in vadose storage and influences some of the groundwaters under elevated flow conditions. The techniques developed in this study may be applied to other karst aquifers where water quality and flow monitoring is taking place.

ACKNOWLEDGMENTS

Funding for this work was provided by the United States Fulbright and David L. Boren international fellowship programs. We gratefully acknowledge A.C.E.G.A. Trieste, Italy and Kraški Vodovod, Slovenia for access to sampling sites. Additional samples were provided by Geokarst Engineering s.r.l., Trieste. The first author was kindly hosted by the Dept. of Environmental Sciences at the Jožef Stefan Research Institute, Ljubljana, Slovenia and the GSF Institute for Hydrology, Neuherberg, Germany during this study. Thoughtful reviews by Paul Hsieh and John Tinsley of the U.S. Geological Survey significantly improved this manuscript.

REFERENCES

Bonacci, O. (1993) Karst springs hydrographs as indicators of karst aquifers. *Hydrological Sciences- Journal des Sciences Hydrologiques*, 38 (1,2), 51-62.

Cancian, G. (1987) L'idrologia del Carso goriziano-triestino tra l'Isonzo e le risorgive del Timavo. *Studi Trentini di Scienze Naturali*, vol. 64, p. 77-98.

Civita, M., Cucchi, F., Eusebio, A., Garavoglia, S., Maranzana, F. & Vigna, B. (1995) The Timavo hydrogeologic system: an important reservoir of supplementary water resources to be reclaimed and protected. Proc. Int. Symp. "Man on Karst", Postojna 1993, *Acta Carsologica*, 24: 169-186.

Deines, P. (1980) The isotopic composition of reduced organic carbon. In: Handbook of Environmental Isotope Geochemistry, Vol. 1 (P. Fritz and J.Ch. Fontes, eds.). Amsterdam: Elsevier, pp. 329-406.

Deines, P., Langmuir, D., and Harmon, R. (1974) Stable carbon isotope ratios and the existence of a gas phase in the evolution of carbonate ground waters. *Geochimica et Cosmochimica Acta*, vol. 38, p.1147-1164.

Doctor, D.H. (2002) The Hydrogeology of the Classical Karst (Kras) Aquifer of Southwestern Slovenia. Ph.D. dissertation, University of Minnesota, 252 pp.

Forkasiewicz, J. and Paloc, H., (1967) Le régime de tarissement de la Foux de la Vis. Etude préliminaire. AIHS Coll. Hydrol. des roches fissurées, Dubrovnik (Yugoslavia), vol. 1, pp. 213-228.

Galli, Mario (1999) Timavo: Esplorazione e studi. Supplemento no. 23 di *Atti e Memorie della Commissione Grotte "Eugenio Boegan"*, Trieste, 195 pp.

Gemiti, F. (1984) La portata del Timavo alle risorgive di S. Giovanni di Duino. *Annali Gruppo Grotte Ass. 30°Ott., Trieste*, 7:23-41.

Gemiti, F. (1994) Indagini idrochemiche alle risorgive del Timavo. *Atti e Memorie della Commissione Grotte "E. Boegan"*, vol. 30, pp 73-83.

Gemiti, F., and Licciardello, M. (1977) Indagini sui rapporti di alimentazione delle acque del Carso triestino e goriziano mediante l'utilizzo di alcuni traccianti naturali. . *Annali Gruppo Grotte Ass. XXX Ott.*, sez. C.A.I. Trieste, 6, 43-61.

Guglia, P. (1994) Risultati esplorativi del Progetto Timavo (1990-1993). *Atti e Memorie della Commissione Grotta "E. Boegan"*, 31/1992-93: 25-48.

Hall, F.R. (1968) Base-flow recessions—a review. *Water Resources Research*, vol. 4 (5): 973-983.

Kranjc, A.,ed., (1997) Slovene Classical Karst-"Kras". Postojna: Institut za raziskovanja krasa ZRC SAZU, 254 pp.

Krivic, P. (1981) Etude hydrodynamique d'un aquifère karstique côtiere: le Kras de Slovenie, Yougoslavie. Accadèmie Montpellier, Univ. Sc. Techn. Languedoc, Thèse de Docteur-Ingénieur Université Montpellier II: 108 pp.

Maillet, E. (1905) *Essai d'Hydraulique Souterraine et Fluviale*. Librarie Scientifique A. Hermann: Paris.

Milanović, P. T. (1981) Karst Hydrogeology. Littleton, Colorado: Water Resources Publications, 434 pp.

Mosetti, F. & D'Ambrosi, C. (1963) Alcune ricerche preliminari in merito a supposti legami di alimentazione fra il Timavo e l'Isonzo. *Boll. Geograf. Teor. ed Appl.*, n. 17.

Sujono, J., Shikasho, S., Hiramatsu, K. (2004) A comparison of techniques for hydrograph recession analysis. *Hydrological Processes*, 18, 403-413.

Tallaksen, L.M. (1995) A review of baseflow recession analysis. *Journal of Hydrology*, **165**: 349-370.

Urbanc, J., and Kristan, S. (1998) Isotope investigation of the Brestovica water source during an intensive pumping test. *RMZ - Materials and Geoenvironment*, vol. 45, no. 1-2, p. 187-191.